Memoirs of the School of Engineering, Nagoya University
Vol.51, No.2 (1999)

COLLECTIVE TRANSLATIONAL-ROTATIONAL COUPLING MOTION OF MOLECULES IN LIQUIDS AND SOLUTIONS

Hiroyasu NOMURA, Shinobu KODA and Tatsuro MATSUOKA

Department of Molecular Design and Engineering, Graduate School of Engineering, Nagoya University

(Received November 11, 1999)

Contents

I. Introduction

In this review, we focus attention upon our recent experimental results of the collective translational and rotational coupling modes of molecular motions in the liquids and solutions. It is very important to elucidate how the molecular site-site interaction does effect on the molecular motions in liquids and solutions, especially to understand the molecular motion of anisotropic molecules at molecular levels. For this purpose, the light scattering and ultrasonically induced spectroscopy techniques are very appropriate and powerful.

The depolarized Rayleigh spectra monitor the fluctuation in the polarizability density that arises from the modulation of the intrinsic and the interaction-induced polarizabilities of the molecules by the molecular motion. In the case of the no-interaction-induced polarizability, the shape of the depolarized Rayleigh spectrum will be determined by the time dependence of the autocorrelation function of a second rank collective orientation density.[1),2)] For symmetric top molecules, the intensity would depend upon the anisotropy in the gas phase polarizability of a molecule and a static orientational correlation parameter given by

$$g_2 = 1 + NX \frac{\langle P_2(i) P_2(j) \rangle}{\langle P_2(i) P_2(i) \rangle} \tag{I-1}$$

where NX is the number of scattering molecules and $P_2(i)$ is a second rank Legendre function of the orientation of molecule i.

In the case of no strong interaction between the normal coordinates on different molecules, the isotropic Raman spectrum reflects vibrational state of a single molecule and gives the autocorrelation function of the phase of the normal coordinate of a single molecule. The anisotropic spectrum gives a correlation function with a second rank spherical harmonic of the molecular orientation. Furthermore, in the absence of intermolecular vibrational-vibrational interactions, it is quite probable that the vibrational and orientational degree of freedom relax independently so that a single-molecule orientational correlation function can be obtained from the Raman spectrum.

In the rotational diffusion limit, the half width of the depolarized light scattering spectra, Γ, give the single-particle orientational correlation function for symmetric tops which is predominantly exponential and characterized by the decay time.[2)]

$$\Gamma^{-1} = \left(\frac{g_2}{j_2} \right) \tau_2 \tag{I-2}$$

where j_2 is a dynamic orientation correlation parameter. At diffusion limit, j_2 and τ_2 are frequency dependent.[3] The orientational correlation time τ_2 can be obtained by Raman band shape analysis and NMR measurement. If g_2 in Eq. (I-2) is almost equal to 1, that is, molecule rotates freely in liquids and solutions, then, $\Gamma^{-1} \sim \tau_2$.

It has been known that in liquids the collective translational and rotational (orientational) modes are strongly coupled. This coupling has been typically observed in a dimensionless transport parameter R which is directly related to the depth of the "Rytov dip" in the VH depolarized Rayleigh scattering, the central dip arising from the coupling of rotation to shear modes.

De Gennes[3] has predicted that the Rayleigh dip could exist in a depolarized light scattering spectrum of liquid crystals in isotropic phase. His theory is based on the phenomenological generalized irreversible thermodynamics and the coupling between orientational and shear modes of molecular motions is expressed by the transport equation using three viscosity parameters, the shear viscosity η_S, the viscosity for relaxation for orientational order ν and the coupling viscosity μ. For this case, the coupling parameter R is expressed by ($R = 2\mu^2/(\eta_S \nu)$) and is directly related to the depth of the "Rytov dip" in the VH depolarized Rayleigh scattering. His phenomenological treatment was confirmed by depolarized light scattering,[4] electric birefringence,[5] flow birefringence[6] and complex shear modulus measurements.[7]

According to de Gennes' phenomenological theory of strong coupling system, the rate of change of the tensor orientational order parameter $Q_{\alpha\beta}$ is defined as

$$R_{\alpha\beta} = \frac{\delta Q_{\alpha\beta}}{\delta t} . \tag{I-3}$$

The conjugated force $\phi_{\alpha\beta}$ can be derived from the free energy F.

$$\phi_{\alpha\beta} = -\frac{\partial F}{\partial Q_{\alpha\beta}} = -A Q_{\alpha\beta} \tag{I-4}$$

where A is the quadratic expansion coefficient of free energy in $Q_{\alpha\beta}$. In the linear region and if the difference between $\delta Q_{\alpha\beta}/\delta t$ and partial derivative $\partial Q_{\alpha\beta}/\partial t = \dot{Q}_{\alpha\beta}$ is negligible, the linear Onsager symmetry equation can be written as

$$\begin{aligned} \sigma^{a}_{\alpha\beta} &= 2\eta_S A_{\alpha\beta}{}^{a} + 2\mu R_{\alpha\beta} \\ \phi_{\alpha\beta} &= 2\mu A_{\alpha\beta}{}^{a} + \nu R_{\alpha\beta} \end{aligned} \tag{I-5}$$

In this case, $\sigma^{a}_{\alpha\beta}$ is anisotropic part of the viscous stress tensor and $A_{\alpha\beta}{}^{a}$ is the anisotropic part of strain rate tensor. The above coupling effect yields complex shear viscosity as[7]

$$\begin{aligned} \eta'_S(\omega) &= \eta_S \left(1 - R \frac{(\omega/\Gamma)^2}{1 + (\omega/\Gamma)^2} \right) \\ \eta''_S(\omega) &= \eta_S R \frac{(\omega/\Gamma)}{1 + (\omega/\Gamma)^2} \end{aligned} \tag{I-6}$$

where Γ is the relaxation frequency of tensor order parameter.[3),7)]

Flow birefringence experiment should also yield R. In flow birefringence, one measures R/Γ, which is virtually independent of boundary conditions, wheresas in light scattering one measures R and Γ independently.

The simple theories that lend themselves to experimental verification with a minimum number of adjustable parameter assume that the viscosity η_S, the reorientational correlation frequency Γ, and the coupling parameter R are evaluated in the k, $\omega \to 0$ limit.[9)-11)] Only adjustable parameter in fitting of the "Rytov dip" is the coupling parameter R.

In this limit, the Γ and R that enter VH scattering and flow birefringence experiments can be used to analyze phenomena for HH light scattering and ultrasonically induced birefringence experiments.[12),13)] In few cases, the translational-rotational coupling parameter affects on the HH light scattering spectrum, but, for situations where the Rytov dip is small, the weak Brillouin side-peaks observed in the HH spectrum provide a better method of measuring R than does the dip in the VH spectrum.

However, the developments of laser light systems and ultrasonic techniques has open a way to measure the ultrasonically induced birefringence directly as a function of ultrasonic frequency and their intensity.[14)-16)] Therefore, it is a very useful techniques to investigate the collective translational and rotational coupling modes of molecular motions in liquids and solutions.

We have constructed and improved the following two experimental systems.

(1) The depolarized light scattering measurement system with a light beating scattering method based on an optical heterodyne technique newly constructed.[17),18)] The laser light are split into two beams which are imposed at the specimen; one beam is an incident light and the other as a reference for heterodyne detection. A half wave plate put in the path of the reference beam rotates its polarization plane by 90° so that the depolarized VH scattering can be detected. The polarized VV scattering and the depolarized VH scattering can be observed alternately with very high accuracy.

(2) The difference of refractive index, $\Delta n = n_{\parallel} - n_{\perp}$, was measured in an ultrasonically induced birefringence experiment, where $n_{\parallel}$ and $n_{\perp}$ are refractive indexes parallel and perpendicular to the direction of sound propagation, respectively. The light from a He-Ne laser passes through the polarizer with an angle of polarization at 45°, sample cell, $\lambda/4$ plate, and analyzer with a small offset angle β from extinction position. If the acoustic field is applied to solutions, the optical phase retardation δ is produced and the intensity of light passed through the analyzer increases. The optical retardation δ is obtained from the light intensities, I_0 and I_b in the absence of the sound wave with the polarizer and with the analyzer being parallel and perpendicular, respectively. The difference of refractive index can be estimated from the equation $\Delta n = \lambda\ \delta/2\pi d$, where β is the offset angle, d the optical path length and λ the wave length of the light. In order to obtain the orientational relaxation time, the pulsed ultrasonic waves are used and their frequency range is from 5 to 225 MHz.

We would like to summarize in the review our experimental and theoretical results of the translational and rotational coupling parameter R obtained from depolarized light scattering and ultrasonically induced birefringence measurements in liquid crystal and colloidal systems. First, we will summarize our recent work for the translational and rotational coupling parameter R obtained from depolarized light scattering in neat and diluted liquid crystal systems. Second, we will show to some extent the theoretical treatment for ultrasonically and flow birefringence. Finally, we will discuss the our recent results for ultrasonically induced birefringence for liquid crystal, polymer solutions, typical colloidal systems and the concentrated surfactant systems.

II. Experimentals

1. Light Beating Scattering Measurements[17)-19)]

In order to obtain the power spectra of the polarized and depolarized light scattering, a light beating scattering method based on an optical heterodyne technique was used. The block diagram of our experimental system is shown in Fig. II-1.

Although the detail of our system has been reported in the literature,[17)-19)] we briefly describe the experimental system. As a light source, a He-Ne laser operating at 632.8 nm with a power of 50 mW and a multi-longitudinal mode was used and the laser light was split into two beams, which were imposed again at the specimen: one beam is as an incident light and the other as a reference light for heterodyne detection. Only the component of scattered light overlapped the reference beam can generate the beat current at the photodiode. The beat signal was received with a spectrum analyzer, and its intermediate frequency (IF) output was square-law detected and fed to a lock-in-amplifier. This light beating technique provides frequency resolution of 1 kHz. The scattering angle θ was measured accurately as the crossing angle of the two beams. A half wave plate put in the path of the reference beam rotates its polarization plane by 90° in order that the polarized VV scattering be detected. Therefore, the polarized VV scattering and the depolarized VH scattering can be observed alternatively.

The sample cell was set in a brass block whose temperature was controlled within ±0.02°C by circulating the temperature-controlled water. The temperature was measured by the thermister covered with teflon tube immersed in the sample.

Figure II-2 shows the typical polarized and depolarized light scattering spectra of *p*-*n*-pentyl *p*'-cyanobiphenyl (5CB) at temperature from 37.16 to 55.96°C at the scattering angle 6.01°.

As shown in Fig. II-2, the shape of spectrum of VV light scattering were well expressed by Lorentzian curve. The VH light scattering is gradually changed with temperature and at higher temperatures, and the unequivocal Rytov dip is observed.

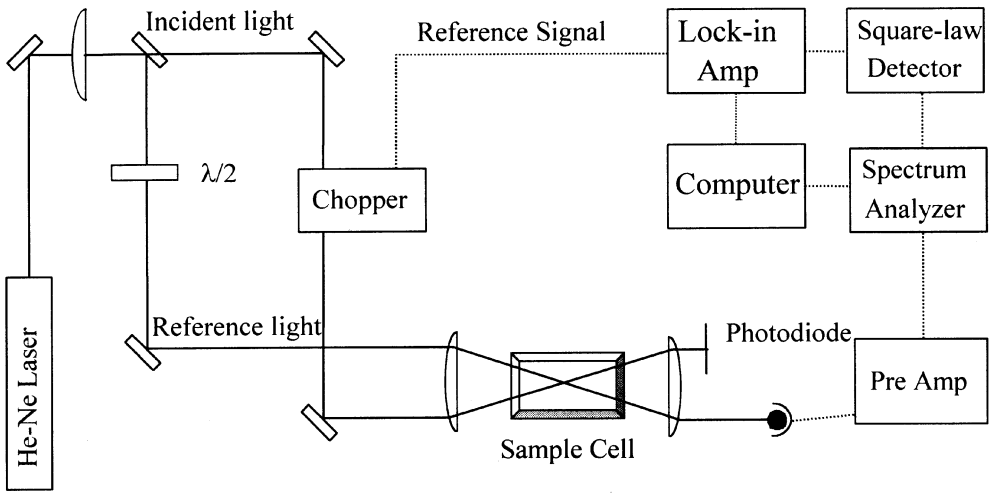

Fig. II-1 Block diagram of Optical beating light scattering method.

A) VV spectra

Molecules of the liquid crystals are in uniaxial shape. In this case, the contribution of orientational fluctuation to the light scattering is predominant and the central component of polarized light scattering spectrum density $I_{VV}(q, \omega)$ can be reproduced as follows when the decay rate of the Brillouin peak and decay rate of reorientation Γ are much smaller than the Brillouin shift ω_B.

$$I_{VV}(q, \omega) = \frac{2\Gamma_R}{\omega^2 + {\Gamma_R}^2} \tag{II-1}$$

where ω is the angular frequency and Γ_R is the half- width at half-height of spectrum and can be written as

$$\Gamma_R = \Gamma - \frac{4}{3}\frac{q^2}{\rho}\eta_S R\frac{\Gamma^2}{\Gamma^2 + \omega_B^2} \tag{II-2}$$

where q is the scattering wave number, ρ is the density and η_S is the shear viscosity. Usually $\omega_B >> \Gamma$ holds so that Γ_R could be equal to Γ. Value of Γ is determined by the usual curve fitting method and the reorientational relaxation times τ are obtained from Γ.

B) VH spectra

The intensity of depolarized light scattering spectrum is expressed by

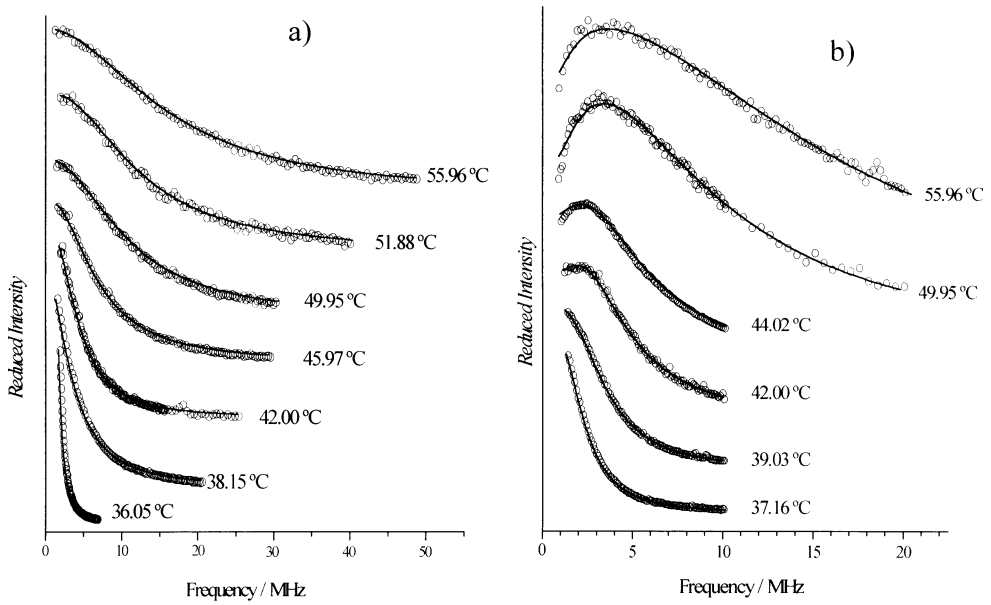

Fig. II-2 Typical light scattering spectra observed in neat 5CB; (a) VV spectra (b) VH spectra. The experimental results are shown by solid circles and calculated results are shown by solid lines. Each Figure. on the right side of spectrum refers to temperature (°C) of measurement. Scattering angle is 6.01°.

$$I_{VH}(q,\omega)=\frac{2\Gamma}{\omega^2+\Gamma^2}\sin^2\frac{\theta}{2}+\frac{2\Gamma\left\{\omega^2+\left(\frac{\eta_S}{\rho}q^2\right)^2(1-R)\right\}}{\left\{\omega^2-\Gamma\left(\frac{\eta_S}{\rho}q^2\right)\right\}^2+\omega^2\left\{\Gamma+\left(\frac{\eta_S}{\rho}q^2\right)(1-R)\right\}^2}\cos^2\frac{\theta}{2} \quad \text{(II-3)}$$

The scattering wave number q is expressed by the following equation;

$$q=\frac{2\pi}{\lambda}\sin\theta \quad \text{(II-4)}$$

where λ is the wave length of incident light and θ is the scattering angle.

The coupling parameter R can be obtained by usual curve fitting method. Data analysis of the depolarized spectra was carried out for all Γ values. Errors in numerical values of Γ were less than 3%. The solid lines in Fig. II-2 are the ones reproduced using the values of viscosity η_S and the obtained coupling parameters R. The agreement between the observed and reproduced results is excellent.

2. Ultrasonically Induced Birefringence Measurement[15),16),20),21)]

To measure ultrasonically induced birefringence, two different detecting techniques were used. One is the "non-biased" measurement[21)] and the other is the "biased" measurement.[15),20)] Figure II-3 shows block diagram of experimental system.

The direction of the incident light is perpendicular to the direction of the sound wave propagation. The light from a He-Ne laser (632.8 nm, 5 mW) passes through the polarizer with an angle of

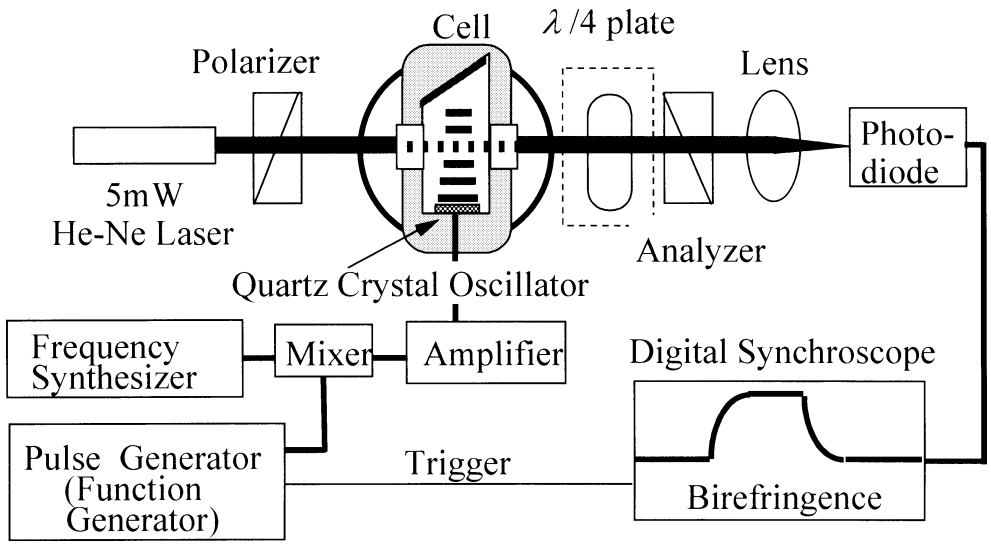

Fig. II-3 Block diagram of ultrasonically induced birefringence measurements.

polarization at 45°, sample cell, and analyzer. For non-biased detection, an analyzer is set at extinction angle. For biased detection, a quarter wave plate is inserted and the analyzer is set with a small offset angle β from its extinction position. If the acoustic field is applied to solutions, the optical phase retardation (is produced and the intensity of light passed through the analyzer increases. For $|\beta| << 1$ and $|\delta| << 1$, the intensities of light passed through the analyzer are given by

$$I = I_0 \left((\delta/2)^2 + \beta\delta + \beta^2 \right) + I_b \tag{II-5}$$

where I_0 and I_b are the light intensities in the absence of the sound wave with the polarizer and the analyzer being parallel and perpendicular, respectively. For the non-biased detection, $\beta = 0$, the phase retardation is given as,

$$\delta = 2\sqrt{\frac{I - I_b}{I_0}} \tag{II-6}$$

while for the biased detection, the phase retardation is given as,

$$\delta = \frac{I_+ - I_-}{2 I_0 \beta} \tag{II-7}$$

where the light intensities with offset angles $\pm\beta$ are described by I_+ and I_-, respectively. The birefringence Δn is related to the phase retardation δ as follows.

$$\Delta n = \frac{\lambda\delta}{2\pi d} \tag{II-8}$$

where d is the optical path length.

The ultrasonically induced birefringence from two different origins exists. One is the sinusoidal birefringence which is proportional to the ultrasonic amplitude that is, the square root of the ultrasonic intensity. The other is the stationary birefringence that is proportional to the ultrasonic intensity. As indicated in Eqs. (II-6) and (II-7), the phase retardation obtained by the non-biased measurements is the root mean square one and thus the sign of birefringence cannot be obtained. The merit of this method is that both the sinusoidal and stationary term can be detected. The Δn in the order of 10^{-8} can be detected. In the biased measurement, the sinusoidal birefringence is averaged and only the stationary component is observed. In this case, the sign of the birefringence can be obtained and high signal to noise (S/N) ratio can be realized if values of β are properly set as $|\delta| << |\beta| << 1$. The Δn in the order of 10^{-11} can be measured and we can distinguish the weak stationary birefringence against the sinusoidal one.

If the birefringence is stationary, the reorientational relaxation time τ is obtained by analyzing the extinction curve. If the reorientational motion is expressed in terms of a single relaxation process, the extinction curve of the birefringence is given as

$$\Delta n(t) = \Delta n_{max} \exp(-t/\tau) \tag{II-9}$$

where Δn_{max} the maximum value of $\Delta n(t)$.

Figure II-4 shows the typical trace of ultrasonically induced birefringence signal for the α-hematite (Fe_2O_3) sol using the biased measurement technique and the waveform of the ultrasonic

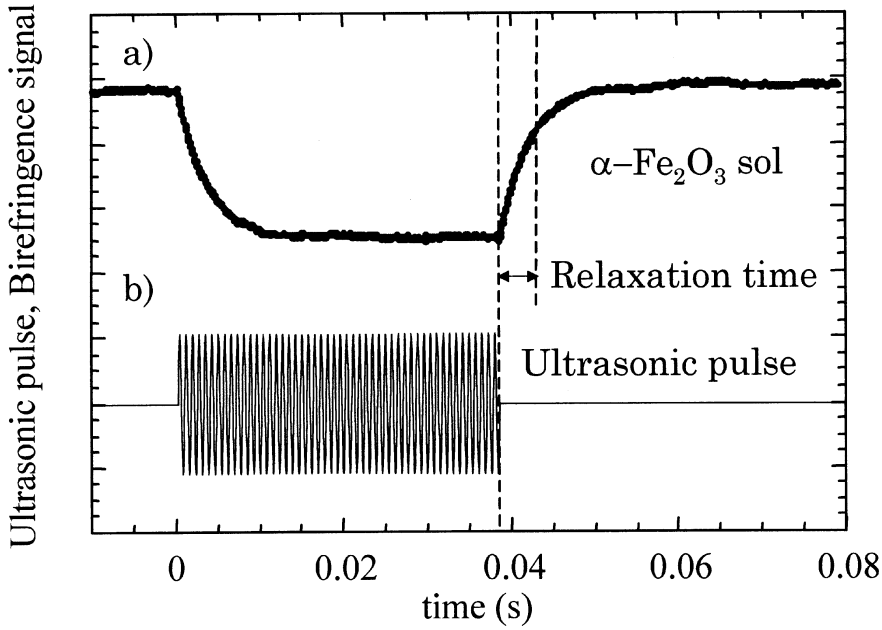

Fig. II-4 (a) Trace of transient ultrasonically induced birefringence of α-Fe_2O_3 sols at volume fraction 4.7×10^{-6} at 25°C (25 MHz, 0.005 W·cm^{-2}). (b) Applied ultrasonic pulse.

pulse used. The sign of the birefringence is negative.

To discuss the frequency dependence of the birefringence, the ultrasonic intensity must be measured precisely. To do so, we measured the ultrasonic intensity on the basis of the light diffracted by the propagating sound waves. The Raman-Nath parameter v_R is defined as,

$$v_R = \frac{2\pi d}{\lambda}\left(\frac{\partial n}{\partial \rho}\right)\delta\rho, \tag{II-10}$$

where n is the refractive index and $\delta\rho$ is the density perturbation caused by ultrasound. The Raman-Nath parameter can be estimated from the diffracted light intensity using the numerical calculation given by Klein and Cook.[22] The Raman-Nath parameter is related to the ultrasonic intensity W_U as,

$$W_U = \frac{{c_0}^3}{2\rho}\left(\frac{\lambda}{2\pi d}\right)^2\left(\frac{\partial \rho}{\partial n}\right)^2 {v_R}^2 \tag{II-11}$$

where c_0 is the sound velocity. The value of $(\partial n/\partial\rho)$ was estimated from an empirical formula given by Gibson and Kinkaid,[23]

$$\rho\left(\frac{\partial n}{\partial \rho}\right) = \frac{(n-1)(n^2+1.4n+1.4)}{n^2+0.8n+1} \tag{II-12}$$

or by Lorentz-Lorenz equation,

$$\rho\left(\frac{\partial n}{\partial \rho}\right) = \frac{(n^2 - 1)(n^2 + 2)}{6n} \tag{II-13}$$

III. Translational and Rotational Coupling Parameter R[17)]

1. Introduction

A number of studies for molecular motions in liquid state have been carried out by light scattering measurements. For many liquids which consist of optically anisotropic molecules, a dip near the central frequency in the depolarized spectrum called the Rytov Dip, is observed. The spectrum has been well understood with the microscopic "two variable" theories which were proposed by several authors.[1),9),10),24)-27)] In the theories, the Rytov dip originates from the coupling between orientational and shear modes of molecular motions in liquid state. To express the Rytov dip quantitatively a coupling parameter R has been introduced as a measure of the coupling. The value of the coupling parameter is determined by the analysis of the depolarized light scattering spectrum with the Rytov dip.

After the theoretical works,[1),9),25),26)] the Rytov Dip in the depolarized spectrum $I_{VH}(\omega)$ have been observed in certain neat liquids such as aniline, nitrobenzene, quinoline, hexadfluorobenzene and *p*-methoxybenzylidene-*n*-butylaniline (MBBA) in isotropic phase etc. Furthermore, the temperature and pressure dependence of the coupling parameter R also has been observed. Values of R in the literatures are summerized in Table III-1 and Fig. III-1. The general features of the coupling parameter R of liquids state are the followings;

(1) The values of the coupling parameter R in liquids state are almost around 0.4, independent of the molecular structure.
(2) The R did not depend on the temperature around in range and the pressure.
(3) Solvent effect, that is viscosity and concentration of diluent, still are obscure because of the limits of experimental accuracy.

Alms *et al.*[27)] measured the depolarized light scattering spectra of *p*-methoxybenzylidene-*n*-butylaniline (MBBA) over the temperature range of 150–230°C and estimated the coupling parameter R. They have reported that the coupling parameters obtained were independent of temperature in the temperature ranges investigated. On the contrary, Kawamura *et al.*[7)] measured the complex shear modulus as a function of temperature and discussed the temperature dependence of the three viscosity parameters of *p*-*n*-pentyl *p*'-cyanobiphenyl (5CB) and MBBA.

Recently, Matsuoka *et al.*[18)] have observed the spectra of depolarized light scattering for *p*-*n*-hexyl *p*'-cyanobiphenyl (6CB). They adopted a new optical beating light scattering technique to observe the Rytov dip near the phase transition point. In comparison with the conventional light scattering technique with the Fabry-Perot interferometer, the new beating technique gives us more accurate depolarized light scattering spectra of liquids.

Comparing with the ordinary liquids such as aniline, nitrobenzene, quinoline and tripenylphosphite, the liquid crystal samples have some advantages; (1) a liquid crystal molecule is uniaxial rigid and anisotropic. (2) In the low temperature, liquids crystal takes a nematic ordered structure, but above the phase transition temperature, they are in isotropic liquids state. By changing the temperature near the phase transition point, we can change the liquid structure locally in bulk liquids. (3) In the isotropic phase far from the transition temperature, liquid crystals can be considered as purely isotropic ordinary liquids, because of their viscosity likely to usual ones. (4)

By addition of the diluent solvent to liquid crystal even in isotropic phase, we are able to obtain the information about how solute (liquid crystal) and solvent (diluent) interaction affect and the local structure changes on the coupling parameter *R*.

We used the liquid crystal samples, 5CB and MBBA. They were purchased from B.D.H Co.

Table III-1 Values of *R* in the literatures.

Sample	R	Temperature range (°C)
MBBA[a)]	0.36 ± 0.02	150 ~ 230
Benzonitrille[b)]	0.37 ± 0.02	–10 ~ 20
Anisaldehyde[c)]	0.43 ± 0.02	6 ~ 79
Salol[d)]	0.28 ± 0.04	65 ~ 122
Acetophenone[e)]	0.43 ± 0.04	–22 ~ 20
Pyridine[f)]	0.35 ± 0.08	–55 ~ 25
Triphenyl Phosphite[g)]	0.45 ± 0.05	–2 ~ 79
Ethyl benzene[h)]	0.41 ± 0.05	–56.5 ~ 33.5
Carbon disulfide[i)]	0.35 ± 0.06	–111 ~ –81

a) Ref. 27, b) Ref. 35, c) Ref. 11, d) G. Enright and B. P. Stoicheff, J. Chem. Phys., **64**, 3658 (1976), e) P. Sixou, P. Bezot and G. M. Searby, Mol. Phys., **30**, 1149 (1975), f) G. M. Searby, P. Bezot and P. Sixou, J. Chem. Phys., **64** 1485 (1976), g) Ref. 45, h) P. Bezot, G. M. Searby and P. Sixou, J. Chem. Phys., **62**, 3813 (1975), i) G. Enright and B. P. Stoicheff, J. Chem. Phys., **60**, 3536 (1974).

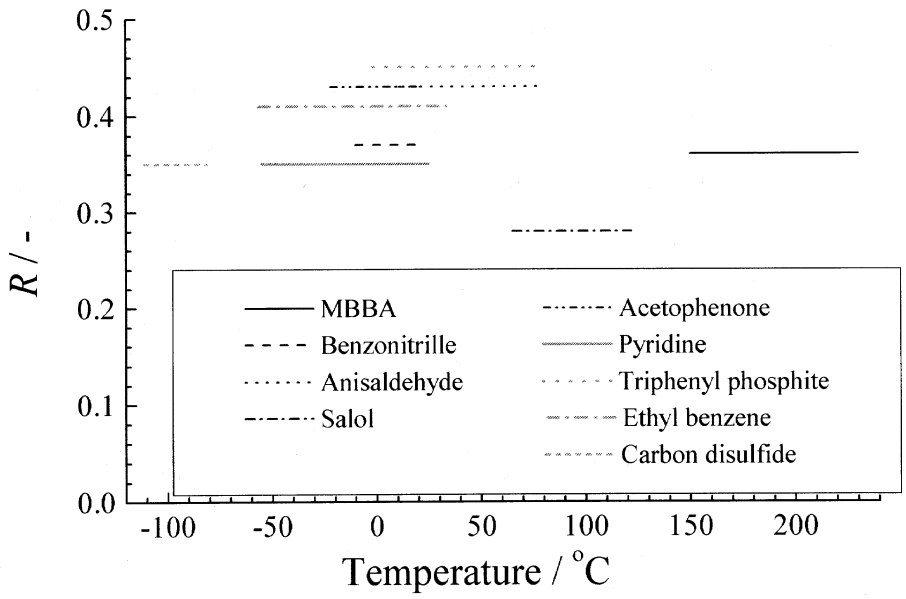

Fig. III-1 Values of *R* in the literatures.

Ltd. and Tokyo Kasei Co. Ltd. respectively and used without further purification. The phase transition temperatures are 35.3 and 46.7°C for 5CB and MBBA, respectively. We used freshly provided samples because the phase transition temperature of these liquid crystals slightly changed gradually with aging. The measuring temperature ranges were from 35.8 to 62.0°C and from 47.7 to 65.6°C each for 5CB and MBBA. As dilulent, carbon tetrachloride and triphenylphosphite were chosen by reasons of their non-polar, spherical and non-spherical properties. Especially, triphenylphosphite (TPP) showed the Rytov Dip in depolarized light scattering measurement.

2. Theoretical Background

Appearance of the Rytov dip can be explained by the two variable theory. Alms *et al.*[27] compared the microscopic two variable theory. with the de Genne's phenomenological theory, and found the relation between the coupling parameter R and the de Gennes' three viscosity parameters,[3] $R = 2\mu^2/(\eta_S \nu)$. According to the two variable theory, the coupling parameter R between translational and orientational modes of molecular motions in liquid state has been expressed as follows:

$$R = \frac{m}{\rho \eta_S \Gamma N k_B T \left\langle \left| \zeta_{xz} \right|^2 \right\rangle} \left| \int_0^\infty \left\langle \tilde{\sigma}_{xz}^{+}(t)\, \dot{\tilde{\zeta}}_{xz}^{*}(0) \right\rangle dt \right|^2 \tag{III-1}$$

where ρ is the density, η_S is the shear viscosity, Γ is decay rate of reorientation, N is the number of molecules, T is the temperature, k_B is the Boltzmann constant, m is the molecular mass and

$$\tilde{\sigma}_{xz} = -\frac{\rho}{q} \sum_i \dot{v}_x(i) \exp(-iqz_i) \tag{III-2}$$

$$\tilde{\zeta}_{xz} = \sum_i \zeta_{xz}(i) \exp(-iqz_i) \tag{III-3}$$

where

$$\zeta_{xz}(i) = \mu_{xi}\, \mu_{zi} \tag{III-4}$$

expresses the orientation of the i th molecule in the laboratory xz frame, μ_{xi} is the x component of a unit vector along a certain axis of the i th molecule, μ_{zi} is the z component, q is the wavenumber and $v_x(i)$ is the velocity i th molecule in the laboratory xz frame.

On the other hand, Alms *et al.*[27] have derived the following expressions for the uniaxial molecule such as liquid crystal:

$$\Gamma^{-1} = g_2 \frac{V^* \eta_S}{k_B T} = \tau \tag{III-5}$$

$$\left\langle \left| \zeta_{xz} \right|^2 \right\rangle = \frac{N}{15} g_2 \tag{III-6}$$

V^* is the effective molecular volume of the rotating molecule, τ is the reorientational relaxation time and g_2 is the static pair correlation function expressed as

$$g_2 = 1 + \sum_{i \neq j}^{N} \frac{\left\langle \zeta_{xz}(i)\, \zeta_{xz}^{*}(j) \right\rangle}{\left\langle \zeta_{xz}(i)\, \zeta_{xz}^{*}(i) \right\rangle} \tag{III-7}$$

Using these notations, the coupling parameter R is reduced to the following expression:

$$R = \frac{15 m V^{*}}{\rho (N k_{\mathrm{B}} T)^2} \left| \int_0^{\infty} \left\langle \tilde{\sigma}_{xz}^{+}(t)\, \dot{\tilde{\zeta}}_{xz}^{*}(0) \right\rangle dt \right|^2 \tag{III-8}$$

3. Coupling between the Translational and Reorientational Motion of Molecules in Neat Liquids Crystal in Isotropic Phase

1) Reorientational Relaxation Times τ

The temperature dependence of the reorientational relaxation time is shown in Figs. III-2(a)

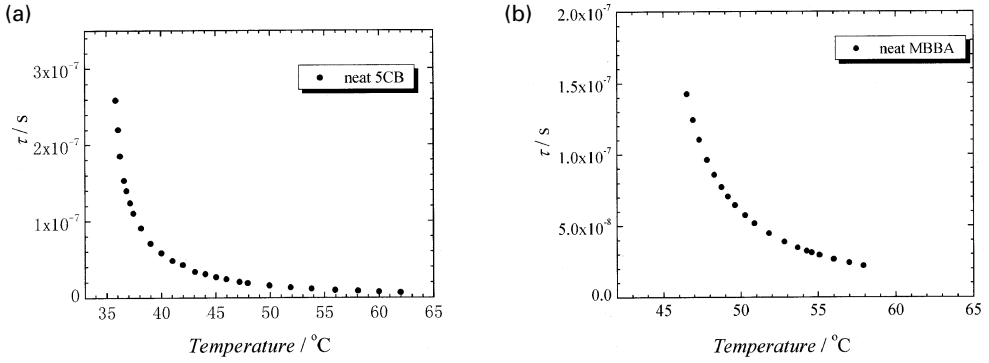

Fig. III-2 Temperature dependence of reorientational relaxation time τ for neat 5CB (a) and neat MBBA (b).

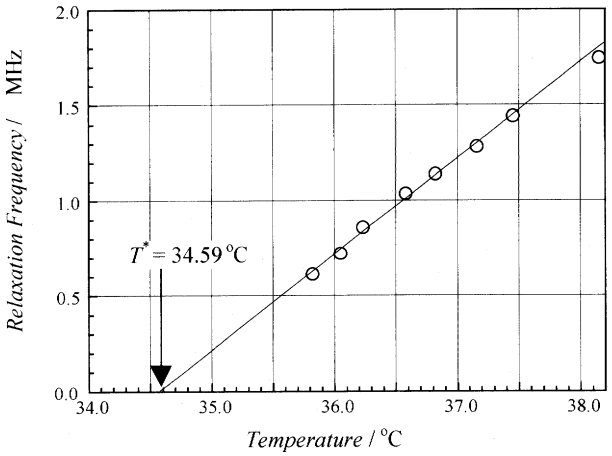

Fig. III-3 Typical example for the determination of transition temperature T^*.

and III-2(b) for 5CB and MBBA, respectively.

Usually the phase transition temperature, T_C is determined as the point at which the milky turbidity of liquid crystal disappears. We extrapolated the plot of between $\Gamma/2\pi$ and T and estimated "the transition temperature T^* as shown in Fig. III-3, because at the temperature the orientational relaxation time will be infinitive, that is $\tau \to \infty$.

2) Coupling Parameter *R* of 5CB and MBBA

The coupling parameter R obtained as a fitting parameter for 5CB and MBBA are plotted against temperature in Figs. III-4(a) and 4(b). As shown in the figures, the values of the coupling parameters R of 5CB and MBBA show a clear temperature dependence near the phase transition temperature, but at the temperature far from the phase transition point, the coupling parameter R also are independent of the temperature likely to ordinary liquids of anisotropic molecules such as aniline, nitrobenzene, etc.

For most experimental results for ordinary liquids such as aniline, nitrobenzene, quinoline etc., the coupling parameter R is independent of temperature.[27] It means that

$$\left| \int_0^\infty \left\langle \tilde{\sigma}_{xz}^{+}(t)\, \dot{\tilde{\zeta}}_{xz}^{*}(0) \right\rangle dt \right|^2 \propto T^2 \qquad \text{(III-9)}$$

Interpretation of this term on molecular level has not been obtained, but Eq. (III-9) indicates correlation between stress and angular velocity in the highly strong collective motion of liquids. The static pair correlation function g_2, even if a static feature, reflects the collective properties of molecular motions in liquid state. If the reorientational motion of each molecule is independent of the motion of other molecules in liquid state, then, g_2 should be unity and Eq. (III-5) reduces to the Debye-Einstein equation.

3) Effects of Reorientaional Relaxation Time and Coupling Parameter on Long Range Order of Isotropic Liquids

It is well known that near nematic phase transition point of liquid crystal, the strong correlation in reorientational motion of molecules exists. After comparing the two variable theory with the de Gennes' phenomenological theory, Alms *et al.*[27] derived the following relation;

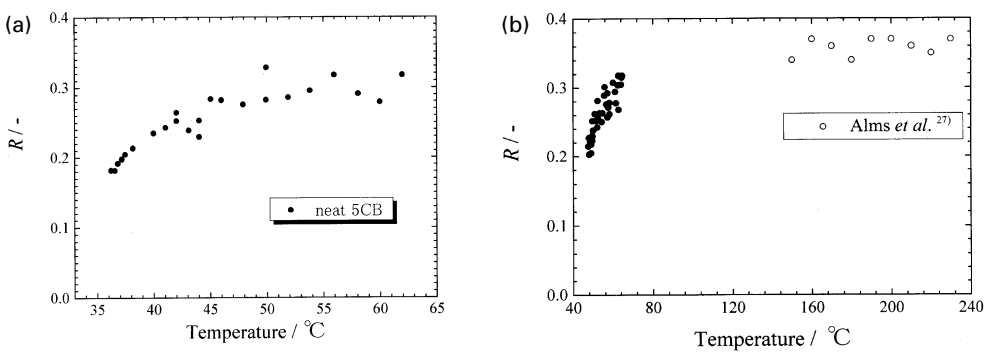

Fig. III-4 Temperature dependence of the coupling parameter R for (a) neat 5CB and (b) neat MBBA.

$$g_2 = \frac{T}{T - T^*} = 1 + \frac{T^*}{T - T^*} \qquad \text{(III-10)}$$

In Fig. III-5, the reorientational relaxation time τ obtained is plotted against the dynamic parameter $\eta_S g_2/T$ (Eq. (III-10) is used). For both cases of 5CB and MBBA, appreciable deviations from the linear relations between τ and $\eta_S g_2/T$ are observed near the phase transition temperature.

The effective volumes V^* for each sample at high temperature limit (197Å^3 for 5CB, 225Å^3 for MBBA) were estimated from the limiting slope of the dotted lines in Fig. III-5. The calculated values of the effective volume for MBBA under the slip and stick boundary conditions are 286 and 220Å^3, respectively using the values of molecular dimension given in literature.[11] The value of V^* obtained in this study is comparable with those calculated.

No theory has been developed for the temperature dependence of coupling parameter R. The theoretical relation between the coupling parameter R and the static pair correlation g_2 is unclear. However, in view of the discussion of the relation of τ to g_2, a relation between the coupling parameter R and the static pair correlation function g_2 of liquid crystal is tentatively examined.

Figure III-6 shows the relation between the coupling parameter R and g_2 obtained from Eq. (III-10) in a double-logarithmic plot.

As is seen in Fig. III-6, the clear linear relations are obtained both for 5CB and MBBA. In the Figure, the values of R for MBBA which were obtained by Alms *et al.* are also plotted. Although the coupling parameters R of MBBA reported by them are independent of temperature, their measuring temperature range is limited and their data approximately fall on our line obtained for MBBA. This means that at least for liquid crystals, the coupling parameter R depends on the degree of correlation in isotropic phase.

The temperature dependences of the coupling parameter for liquid crystals, 5CB and MBBA in the isotropic phase were obtained from the polarized and depolarized Rayleigh light scattering

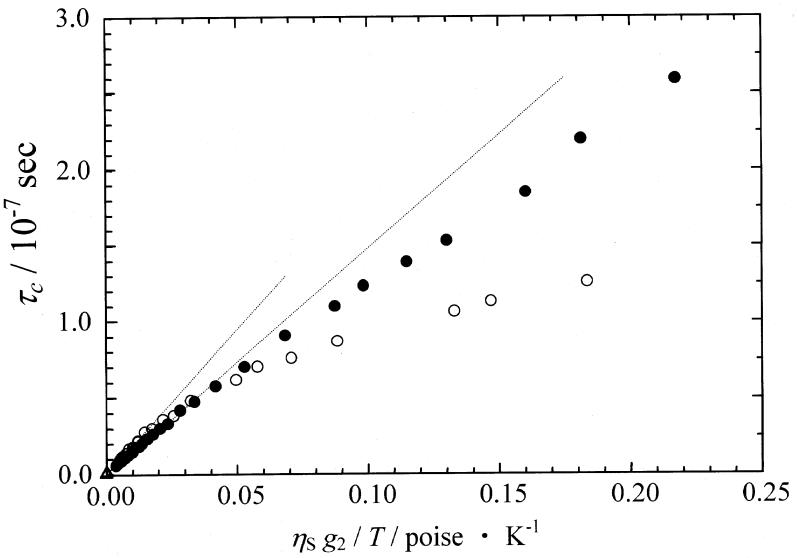

Fig. III-5 τ plotted against $\eta_S g_2/T$ for the both samples. Solid circle, 5CB; open circle, MBBA. The dotted lines indicate the limiting slope for each sample at high temperature limit.

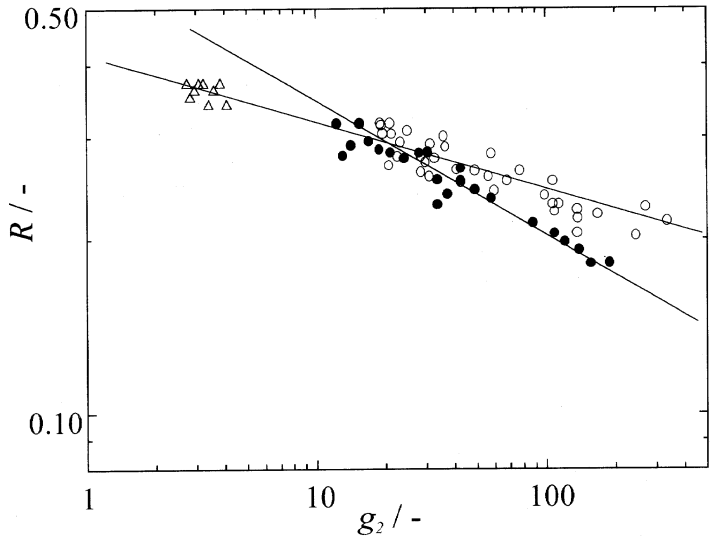

Fig. III-6 *R* plotted against g_2 for the both samples. Solid circle, 5CB; open circle, MBBA; and open triangle, from Ref. 27. The solid lines are drawn schematically for ease of comprehension.

spectra. At temperatures far above the nematic-isotropic phase transition point, the parameter *R* was independent of the temperature. As the temperature approaches the transition point, the value of the coupling parameter *R* decreased from a constant value at temperatures high above the transition point. Similar behavior was also observed for 6CB by Ueno *et al.*[28] These indicate that the coupling parameter *R* depends on the long-range orientational order as well as on the local structure in the liquid state. The addition of non-liquid crystal molecules should affect the local structure of the liquid crystal molecules.

4. Effects of Diluent on the Coupling Parameter *R*[29),30)]

1) Introduction

In order to have a deep understanding of the coupling mechanism between reorientational and translational motion of molecules, information of molecular interaction is highly important. Therefore, it is very useful to observe the mixing effect of the diluent on the coupling parameter *R*. Several results were reported on the effects of the diluents on the coulping parameter *R* for mixtures of non-liquid crystal systems.[26),31)] Because of the experimental difficulties arising from limited resolution of the Fabry-Perot interferometer the discussions are still obscure.

Isotropic phase of liquid crystal is very appropriate for the study of the coupling between translational and rotational modes of molecules. The reasons are as follows: 1) The molecular shape is uniaxial and their reorientational pair correlation changes strongly with temperature; 2) the reorientational relaxation frequency is large enough to use the light scattering technique based on optical beating detection which, with its very high frequency resolution, enables us to carry out a precise measurement of coupling parameter.

In this section, we will discuss diluent effect on the coupling parameter of 5CB and MBBA in the mixed system as a function of temperature. As diluent, we chose carbon tetrachloride (CCl_4) and triphenyl phosphite (TPP). Carbon tetrachloride is a non-polar and spherical molecule and its

miscibility for 5CB is poor but for MBBA fairy good. On the contrary, TPP is a nearly symmetric top molecule and quite miscible with 5CB. Besides, the Rytov dip has been observed in neat liquid TPP.[8),32)]

In addition, we will also discuss the temperature and diluent concentration dependence of the coupling parameter *R* by combining with the information of local structure of 5CB and its mixture in isotropic phase obtained by the NMR and Raman scattering measurements.

2) Diluent Effect on Phase Transition Temperature

It is well known that the phase transition temperature is lowering by addition of the diluent. The concentration dependences of the phase transition temperature *T** obtained from extrapolating to $\Gamma/2\pi \rightarrow 0$ are summarized in Fig. III-7.

As shown in Fig. III-7, the concentration dependences of *T** are different in the 5CB-CCl_4, 5CB-TPP and MBBA-CCl_4 mixtures. In the 5CB-TPP and MBBA-CCl_4 mixtures, *T** decreases with increasing concentration of diluent TPP and CCl_4 in the mixtures. Similar concentration dependence of *T** was reported by Gierke and Flygare.[4)] The value of *T** in their paper for neat MBBA is lower than those reported by other researchers[6),7),33),34)] which are around 41.55–44.3°C, but the concentration dependence curve of *T** is in good agreement with our results. On the contrary, in 5CB-CCl_4 mixtures, the phase transition temperatures are almost independent of the CCl_4 concentration in the mixtures below about 10 mole%. In addition, in our experiments, we noticed the phase separation in 5CB-CCl_4 mixtures just below the temperature *T**. From these results, we may consider that the miscibility of carbon tetrachloride to 5CB is very poor. The reason is as follows: the 5CB molecule is rod-like, highly rigid and highly polarizable, while the CCl_4 molecule is spherical and non-polar. Because of the low miscibility of CCl_4 with 5CB near the phase transition temperature, the interaction between 5CB molecules is so strong, even in the isotropic phase, that CCl_4 molecules can not penetrate the space around the 5CB molecules; however, at temperatures far above the phase transition, 5CB molecules rotate more actively and the anisotropy due to molecular interaction diminishes.

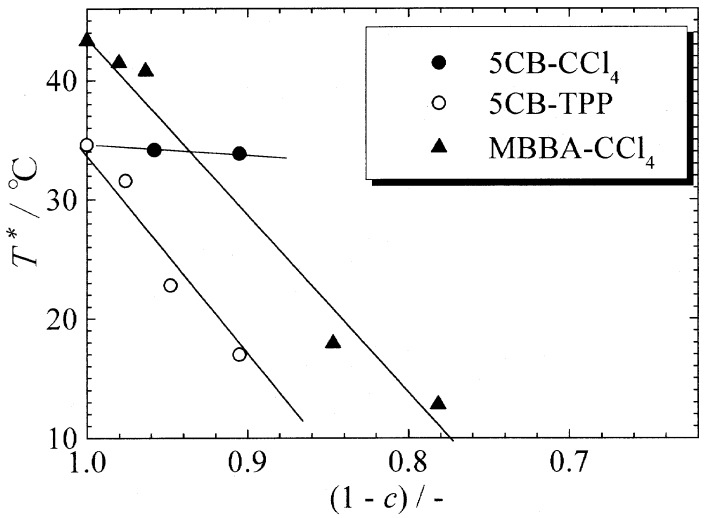

Fi. III-7 Concentration dependence of the transition temperature *T** for 5CB-CCl_4, 5CB-TPP and MBBA-CCl_4 mixtures.

3) Concentration Dependence of Reorientaional Relaxation Time

The reorientational relaxation time obtained by light scattering can be expressed in terms of two factors; one is the single particle reorientational relaxation time and the other the orientational pair correlation function.[35] As seen in Figs. III-8(a), 8(b), and 8(c), the reorientational relaxation time τ depends strongly on the change in phase transition temperature arising from the addition of the diluents. However, in 5CB-CCl_4 mixture, diluent dependence of τ is very small. On the contrary, in the case for the 5CB-TPP and MBBA-CCl_4 mixture, the τ depends on the concentration of the diluent, but the temperature dependence curves change only slightly in low diluent concentration. Therefore, the effect of addition of diluent on the orientational correlation of liquid crystal molecules in 5CB-TTP and MBBA-CCl_4 mixture is weak in concentrations of liquid crystals less

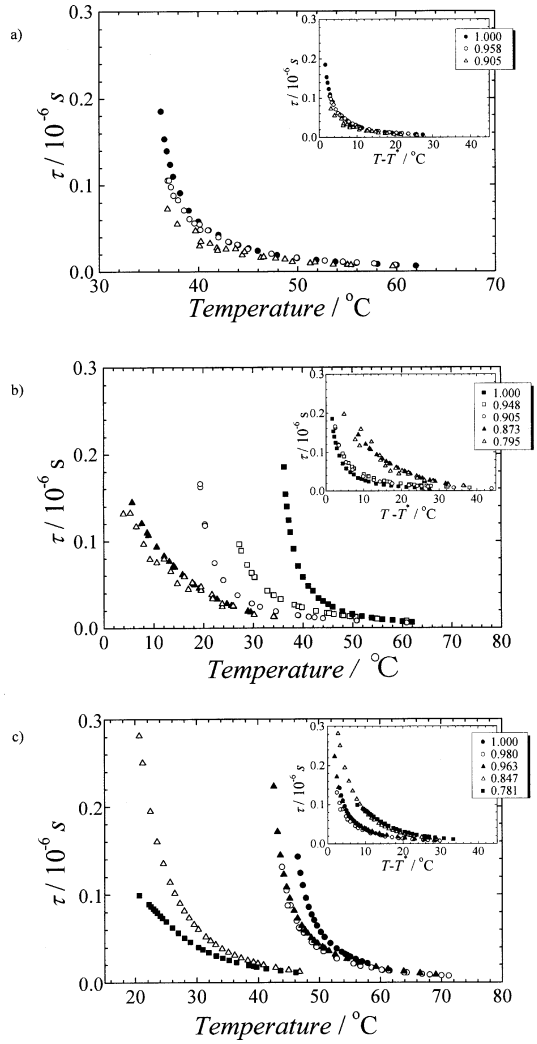

Fig. III-8 Temperature dependence of reorientational relaxation time τ. (a) 5CB-CCl_4, (b) 5CB-TPP, (c) MBBA-CCl_4. Mole fraction of liquid crystals is indicated at right side of each figure.

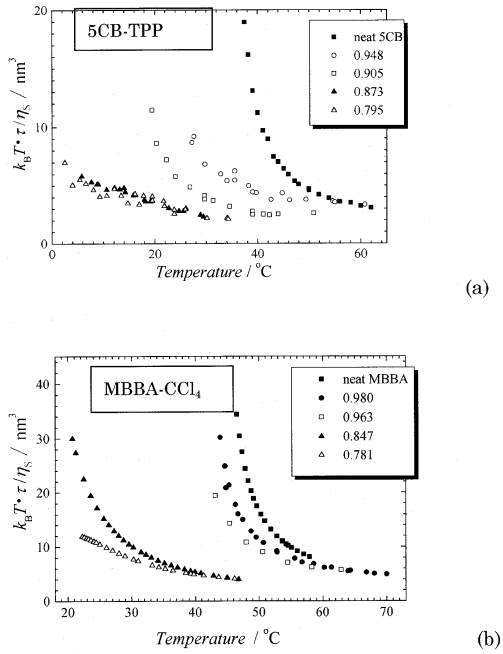

Fig. III-9 Temperature dependence of the $k_BT\cdot\tau/\eta_S$. (a) 5CB-TPP, (b) MBBA-CCl_4. Mole fraction of liquid crystals is indicated at the right side of the each figure.

than 5 mole% in which variation of T^* is less than 10°C.

As shown previously, in isotropic phase of liquid crystal system, the reorientational relaxation time τ can be expressed by Eq. (III-5), where g_2 is the long-range interaction parameter which is also written by Eq. (III-9) and V^* is the molelular volume of liquid crystal. Figures III-9(a) and 9(b) show the temperature dependence of $k_BT\tau/\eta_S$ for 5CB-TPP and MBBA-CCl_4 systems. As shown in Eq. (III-5), the slope of this temperature dependence plot indicates those of g_2V^*. Near the phase transition temperature, the parameter g_2 should be diverse and at temperature far from the transition point, the long range order will disappear, $g_2 \rightarrow 1$, and the values of $k_BT\tau/\eta_S$ should be the molar volume of liquid crystal. As is seen in Fig. III-9(a) and 9(b), in case of 5CB-TPP and MBBA-CCl_4 systems, the slop of the concentration dependence of the $k_BT\tau/\eta_S$ looks to approach to the constant values.

4) Concentration Dependence of the Coupling Parameter *R*

The coupling parameter R obtained is plotted against temperature in Figs. III-10(a), 10(b) and 10(c) for the mixtures of 5CB-CCl_4, and TPP and MBBA-CCl_4, respectively.

As shown in the figures, the difference in temperature dependence of the coupling parameter R for 5CB-CCl_4 mixture and those for 5CB-TPP and MBBA-CCl_4 mixtures, is different, that is, the coupling parameter R of 5CB-CCl_4 mixtures clearly depends on the temperature, but for the 5CB-TPP and MBBA-CCl_4 mixtures, the R values are almost independent of the temperature, as in the case for ordinary liquids of anisotropic molecules.

Because of the low miscibility of CCl_4 with 5CB, the long-range correlation of 5CB molecules is strong and the influence of CCl_4 molecules is weak near the transition point. Therefore,

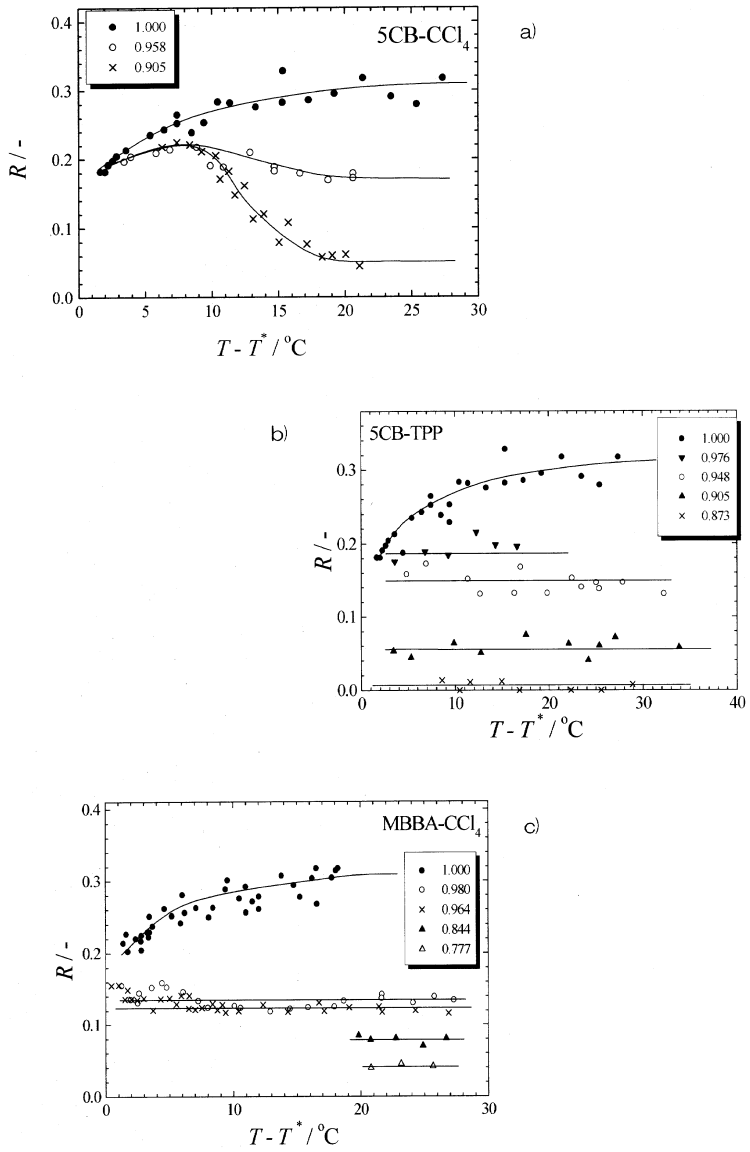

Fig. III-10 The coupling parameter R obtained for various concentrations plotted against T-T*. (a) 5CB-CCl_4, (b) 5CB-TPP, (c) MBBA-CCl_4.

the coupling parameter R of the 5CB-CCl_4 mixture approaches that of neat 5CB. On the other hand, the miscibility of CCl_4 and TPP with MBBA and 5CB, respectively is rather good even near the phase transition temperature, and the CCl_4 and TPP molecules mix well homogeneously. The effect of the long-range interaction on the coupling parameter R is thus weak and R becomes almost independent of the temperature.

On the other hand, as is seen in Fig. III-10(a) and 10(b), the coupling parameters R of both

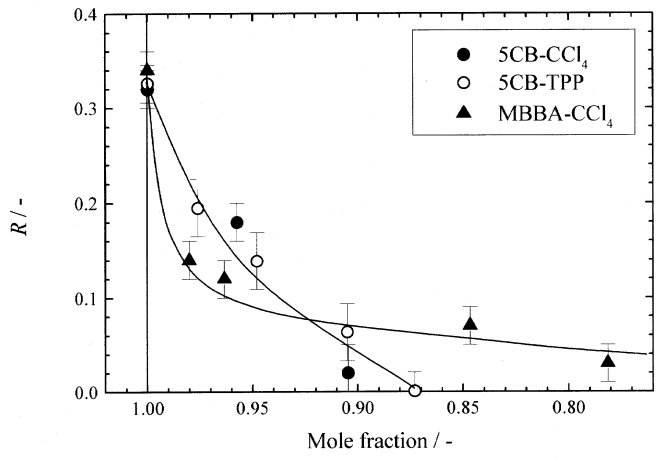

Fig. III-11 The coupling parameters at temperature far above the transition point plotted as a function of concentration of liquid crystals.

liquid crystals in the higher temperature range far from the phase transition are almost independent of the temperature, similar to the ordinary liquids of anisotropic molecules. Furthermore, in Fig. III-11, the coupling parameter of *R* of both 5CB and MBBA mixtures decreases with increasing concentration of diluent. The viscosity of the 5CB-CCl_4 and TPP mixtures decreases with increasing temperature, but is almost independent of the diluent concentration in the low concentration ranges examined here. The diluent dependences of *R* in this work are different from those in benzonitrile mixtures as reported by Whittenburg and Wang.[31] One of the reasons for the difference between ordinary benzonitrile mixtures and liquid crystal mixtures may be their difference in viscosity. In liquid crystal systems, internal factors dominating the viscosity are essentially different from those in the case of ordinary mixtures.

In every case, 5CB-TPP and -CCl_4 and MBBA-CCl_4 mixtures, the coupling parameter *R* decreases with increasing concentration of diluent in the mixtures. However, at higher concentrations of diluent above 5 mole%, we can not determine the coupling parameter *R* from the VH scattering spectra. As is seen in Fig. III-11, it is very interesting that diluent concentration dependences of *R* of 5CB are almost independent of the species of diluent, that is, CCl_4 and TPP but the diluent dependences of *R* are quite different between 5CB and MBBA.

Clear concentration dependence of the coupling parameter *R* suggests that *R* is strongly affected by the local structural change in the mixtures. Furthermore, it was suggested by X-ray diffraction measurements that 5CB molecules are associated, due presumably to their high dipole moments, even in the isotropic phase.[36]

In order to clarify these points, following NMR and Raman scattering measurements have been carried out for the 5CB-CCl_4 and TPP mixtures as a function of temperature.

5) MNR and Raman Scattering Measurements of 5CB-CCl_4 and TPP Systems

5-1) NMR measurement: Chemical shifts of ^1H and ^{13}C of the 5CB molecule were measured for neat 5CB, 5CB-CCl_4, and 5CB-TPP mixtures in the temperature range from 35 to 50°C.

The effects of addition of TPP on the ^1H and ^{13}C chemical shifts were almost the same except for the fact that the chemical shift of the terminal CH_3 group and the CN group are distinctively different between CCl_4 and TPP mixtures.

The chemical shifts σ of neat 5CB, 5CB-CCl_4, and 5CB-TPP mixtures shifted linearly to higher and/or lower field (upfield and/or downfield shift) with increasing temperature. What can be deduced from the NMR measurement are the following:

i) No remarkable differences in $d\sigma/dT$ exist among the chemical shifts of ^{1}H and ^{13}C in 5CB molecule in neat and mixtures.
ii) Increase in temperature gives rise to the downfield shift of the chemical shifts of ^{1}H of the alkyl group and the changes in the middle part of the alkyl groups are remarkable.
iii) ^{13}C chemical shifts of the alkyl group show the upfield shift by the γ-effects with increasing number of the gauche part in the alkyl chain. The result suggests that the motion of the alkyl group becomes more active with increasing temperature for every mixture.
iv) On the contrary, ^{13}C chemical shift of the biphenyl group shows downfield shift. This is attributable to the stacking effects of biphenyl groups. The tumbling motion around the C-C bond between the phenyl groups becomes more frequent with temperature and the co-planner structure of the biphenyl group will be increased.
v) Upfield shift of ^{13}C chemical shift of the terminal CN group may be caused by the interaction with the nearest neighbors around the terminal CN group.

5-2) Raman scattering mesurement: Raman spectra for neat 5CB, 5CB-CCl_4 (10 mole%) and 5CB-TPP (10 mole%) mixtures were obtained as a function of temperature. The observed Raman shifts of each vibration in neat 5CB are in good agreement with those by Gray and Mosley.[37] No difference among the Raman bands in neat and mixtures was observed. Temperature dependence of the three strong Raman shifts, that is, the C-C stretching of aromatic ring, the C-C stretching of biphenyl link and the CN stretching vibration were observed in neat 5CB and 5CB-CCl_4 mixture. These Raman bands shift to lower frequency side with increasing temperature, but the changes in Raman shifts are less than 1 cm^{-1}. These results show that the molecular structure, especially aromatic part of 5CB molecule is not influenced by increase in temperature nor addition of diluent.

The molecule of 5CB consists of the flexible alkyl chain, the rigid biphenyl group and the terminal dipolar CN group. From the temperature and diluent effects of Raman shifts, it is clear thst the molecular structure as a whole does not change. Early in 1975, from the X-ray diffraction experiments, Leadbetter *et al.* suggested the existence of local structure of 5CB molecules in isotropic phase and proposed a model as shown in Fig. III-12.[36] In their model, the 5CB molecules in

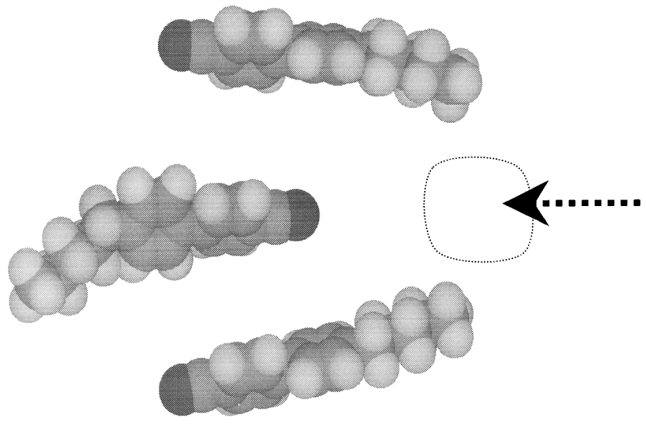

Fig. III-12 Schematic model of the local structure in 5CB proposed by Leadbetter *et al.*

the liquid state are arranged so that their dipoles are anti-parallel and their biphenyl groups are stacked.

Our results of NMR measurements confirmed their model one step further. By addition of diluent, the diluent molecule will approach the dotted region from the outer side as shown in Fig. III-12. Therefore, the ^{1}H and ^{13}C chemical shifts of the terminal methyl and CN group are influenced to an different extent by TPP and CCl_4, respectively.

6) Local Structure and Coupling Parameter

The temperature dependence of coupling parameter *R* of 5CB-TPP MBBA-CCl_4 mixtures and 5CB-CCl_4 mixture can be interpreted as follows; even in the isotropic phase, the local structure of 5CB will exist at any temperature. The temperature dependence of *R* is ascribed to the local structure changes induced by the temperature changes. The local structure changes are related to the miscibility of the diluents. Therefore, the effects of TPP and CCl_4 on the temperature dependence of the coupling parameter *R* of 5CB are different.

The concentration dependence of the coupling parameter *R* in the region far from the transition temperature can be considered as follows; The local structure is influenced by addition of diluent. With loosing the local structure, the coupling parameter *R* will decrease. No difference remains in the miscibility of TPP and CCl_4 with 5CB in the higher temperature region. For this reason the coupling parameter *R* will only depend on the amount of diluent and be independent of the diluent species.

IV. Ultrasonically Induced Birefringence and Coupling Parameter *R*[21] –Theoretical Considerations–

1. Introduction

Birefringence has been observed in some liquids and solutions under the irradiation of longitudinal ultrasounds.[15),20),38)-42)] For large particles of anisotropic shape such as rod like and planar colloidal particles, ultrasonic radiation pressure produces a stationary torque on the particles and induces reorientational order as a whole, because the orientational relaxation frequency of particles is much smaller than that of ultrasound frequency. In this case, the induced birefringence is proportional to the ultrasonic intensity.[15),20),38)-40)] The dynamical properties of large particles can be investigated by following the decay of the birefringence after rapid cessation of ultrasonic irradiation.[15),20),38)-40)]

For neat liquids, however, a sinusoidal velocity gradient can directly produce sinusoidal orientational order. The reorientational order produced is not uniform but propagates as waves and the induced birefringence should be proportional to the ultrasonic amplitude, that is, the square root of the ultrasonic intensity.[12),38),41),42)] In the neat liquids, we cannot obtain the transient decay curve after rapid cessation of ultrasonic irradiation. If the relaxation frequency for reorientational motion is close to the applied ultrasound frequency, the birefringence per amplitude of the applied ultrasonic wave should be affected by the reorientational relaxation processes of the molecules. Measurement of birefringence as a function of frequency gives information of the reorientational motion in liquids.

Problems with regard to the coupling of the reorientational mode to the translational mode have been investigated mainly by flow birefringence and VH depolarized light scattering.[1),3),11),27),43)-48)] Theories for the flow birefringence and the VH depolarized light scattering were constructed independently on the basis of the de Gennes' phenomenological theory[3),27),43),44)] and

irreversible statistical mechanics.[1),2),11),45)-47)] In both theories, the coupling of reorientational mode to the shear mode was taken into account. The expressions derived from both theories are consistent each other.[27)] In the case of ultrasonically induced birefringence, where coupling of the reorientational mode to the longitudinal mode should be taken into account, the formula for the birefringence from the irreversible statistical treatment has already been derived by Lipeles and Kivelson.[48)] The problem of the coupling of reorientational mode to the longitudinal mode should be also taken into account in derivation of the spectra density for the polarized VV and the depolarized VH light scattering. Kivelson and co-workers have extensively investigated the problem from the irreversible statistical mechanics.[32)] Grubbs and MacPhail investigated the line shape of stimulated Brillouin gain spectra and discussed the coupling of the reorientational mode to the longitudinal mode.[49)] Unlike the earlier theory of Lipeles and Kivelson,[48)] they used four independent variables to derive the spectral density for the VV light scattering. On the other hand, Wang derived formulae for the spectrum of density fluctuation of the VV light scattering from the de Gennes' approach.[50)] In this paper, we will present a theoretical expression of the ultrasonically induced birefringence in terms of the de Gennes' phenomenological theory and compare it to that obtained by Lipeles and Kivelson. We also compare our results with the earlier theories.[38),51)-53)]

The isotropic phase of liquid crystals is most appropriate to examine the expression obtained here, because the relaxation frequencies of the orientational motions are the same order magnitude as the ultrasonic frequencies usually used for ultrasonic relaxation studies.[17)] Besides, the flow birefringence for isotropic phase of liquid crystal, 5CB, has been already reported by Martinoty *et al.*[42)] The values of the flow birefringence and the relaxation frequencies are required to reproduce the frequency dependence of the ultrasonically induced birefringence.

2. Theory

Stress induced birefringences in liquids of anisotropic molecules, such as those induced ultrasonically or by flow, can be understood in the theoretical frame work of de Gennes' phenomenological treatment[3),43)] of the coupling of the reorientational order parameter to the strain rate tensor for an anisotropic molecule in liquids and solutions. First, we will present the generalized transport equations taking into account coupling of the orientational order to the strain rate tensor. Secondly, we will discuss the expressions for ultrasonically induced birefringence.

1) Transport Equations

To obtain general expressions for the transport equations, we need the equations of mass and momentum conservation:

$$\delta\dot{\rho} + \rho\partial_k v_k = 0 \tag{IV-1}$$

$$\rho\dot{v}_\alpha = \partial_\beta(\sigma_{\alpha\beta} - \delta p\,\delta_{\alpha\beta}) \tag{IV-2}$$

where ρ is the equilibrium density, $\delta\rho$ and δp are the mass and pressure fluctuations, respectively, $\sigma_{\alpha\beta}$ is the stress tensor and v_α is the velocity vector and repeated indices are summed. For the sake of simplicity, we neglect here the effects of temperature fluctuations. The stress tensor and strain rate tensor, $\sigma_{\alpha\beta}$ and $A_{\alpha\beta}$ can be written as the sum of isotropic and anisotropic parts:

$$\sigma_{\alpha\beta} = \sigma_{\alpha\beta}{}^{\mathrm{i}} + \sigma_{\alpha\beta}{}^{\mathrm{a}} \tag{IV-3}$$

$$A_{\alpha\beta} = A_{\alpha\beta}{}^{\mathrm{i}} + A_{\alpha\beta}{}^{\mathrm{a}} \tag{IV-4}$$

The isotropic and anisotropic parts of the strain rate tensor are respectively written as follows,

$$A_{\alpha\beta}{}^{\mathrm{i}} = \partial_k v_k \, \delta_{\alpha\beta} / 3 \tag{IV-5}$$

$$A_{\alpha\beta}{}^{\mathrm{a}} = (\partial_\alpha v_\beta + \partial_\beta v_\alpha)/ 2 - \partial_k v_k \, \delta_{\alpha\beta} / 3 \tag{IV-6}$$

To consider the coupling of translational mode to reorientational mode, we will use the de Gennes' phenomenological treatment and take the tensor order parameter of molecular reorientation $Q_{\alpha\beta}$ and its conjugated stress $\phi_{\alpha\beta}$ as internal variables.[3),43)] Since the tensor order parameter is anisotropic (i. e. traceless), the anisotropic part of the $\sigma_{\alpha\beta}$ and $A_{\alpha\beta}$ can couple to the reorientational mode. The relation between "force" and "flow" can be thus written by the expression of non-equilibrium thermodynamics as follows:

$$\sigma_{\alpha\beta}{}^{\mathrm{i}} = 3\eta_{\mathrm{V}} A_{\alpha\beta}{}^{\mathrm{i}} \tag{IV-7}$$

$$\sigma_{\alpha\beta}{}^{\mathrm{a}} = 2\eta_{\mathrm{S}} A_{\alpha\beta}{}^{\mathrm{a}} + 2\mu \dot{Q}_{\alpha\beta} \tag{IV-8}$$

$$\phi_{\alpha\beta} = 2\mu A_{\alpha\beta}{}^{\mathrm{a}} + \nu \dot{Q}_{\alpha\beta} \tag{IV-9}$$

where η_{V} is the volume viscosity, η_{S} is the shear viscosity, and μ and ν are viscosity parameters introduced by de Gennes: μ is a measure of coupling between $Q_{\alpha\beta}$ and anisotropic part of the flow field, while ν is related to the relaxation of $Q_{\alpha\beta}$. The dot above $Q_{\alpha\beta}$ denotes taking time derivative.

In the original de Gennes' theory, the strain rate tensor $A_{\alpha\beta} = (\partial_\alpha v_\beta + \partial_\beta v_\alpha)/2$[3),43)] was used in Eqs. (IV-8) and (IV-9). He only dealt with incompressible fluids in which case the relation $A_{\alpha\beta} = A_{\alpha\beta}{}^{\mathrm{a}}$ holds. To extend his treatment to the general case, for example plane sound wave propagation, the anisotropic part of the strain rate tensor should be coupled to the tensor order parameter $Q_{\alpha\beta}$. If the fluctuation of $Q_{\alpha\beta}$ is small, the relation of $Q_{\alpha\beta}$ and $\phi_{\alpha\beta}$ is written as,[3),43)]

$$\phi_{\alpha\beta} = -AQ_{\alpha\beta} \tag{IV-10}$$

where A is the quadratic expansion coefficient of free energy in $Q_{\alpha\beta}$. We also need the following thermodynamic relation,

$$\delta\rho = (\partial\rho / \partial p)_{\mathrm{s}} \delta p = c_0{}^{-2} \delta p \tag{IV-11}$$

where c_0 is the sound velocity in the low frequency limit. From Eqs. (IV-1) to (IV-11), we can deduce the following linearized transport equations,

$$\delta\dot{\rho} + \rho\partial_k v_k = 0 \tag{IV-12}$$

$$\rho\dot{v}_\alpha = \partial_\beta \left(3\eta_{\mathrm{V}} A_{\alpha\beta}{}^{\mathrm{i}} + 2\eta_{\mathrm{S}} A_{\alpha\beta}{}^{\mathrm{a}} + 2\mu \dot{Q}_{\alpha\beta} - \delta\rho c_0{}^2 \delta_{\alpha\beta} \right) \tag{IV-13}$$

$$-AQ_{\alpha\beta} = 2\mu A_{\alpha\beta}{}^{\mathrm{a}} + \nu \dot{Q}_{\alpha\beta} \tag{IV-14}$$

For a longitudinal velocity field with $\partial_x v_x \neq 0$, $\partial_y v_y = \partial_z v_z = 0$, Eq. (IV-12) to Eq. (IV-14) can be written as:

$$\dot{\delta\rho} + \rho \partial_x v_x = 0 \tag{IV-15}$$

$$\dot{v_x} = \frac{1}{\rho}\left(\eta_V + \frac{4}{3}\eta_S\right)\partial_x{}^2 v_x + 2\frac{\mu}{\rho}\partial_x \dot{Q}_{xx} - \frac{{c_0}^2}{\rho}\partial_x \delta\rho \tag{IV-16}$$

$$\dot{Q}_{xx} = -\Gamma Q_{xx} - \frac{4}{3}\frac{\mu}{\nu}\partial_x v_x \tag{IV-17}$$

$$\dot{Q}_{yy} = -\Gamma Q_{yy} + \frac{2}{3}\frac{\mu}{\nu}\partial_x v_x \tag{IV-18}$$

$$\dot{Q}_{zz} = -\Gamma Q_{zz} + \frac{2}{3}\frac{\mu}{\nu}\partial_x v_x \tag{IV-19}$$

where Γ is the relaxation frequency of reorientational order, which is related to ν and A as $\Gamma = A/\nu$. Taking into account the traceless character of the tensor order parameter and the requirement from the longitudinal symmetry, the relations $Q_{xx} + Q_{yy} + Q_{zz} = 0$ and $Q_{yy} = Q_{zz}$ must hold. Eqs. (IV-17) to (IV-19) satisfy these requirements and the transport equations can be written by only three independent variable $\delta\rho$, v_x, and Q_{xx}. Eqs. (IV-15) to (IV-17) are the fundamental equations for the sound propagation and the ultrasonically induced birefringence. The dispersion relation for sound propagation is discussed in the APPENDIX of this section and is compared with Grubbs and MacPhail's treatment based on the irreversible statistical mechanics.

2) Ultrasonically Induced Birefringence

In this section, we will derive an expression for the ultrasonically induced birefringence using the transport equations obtained in the previous section. Birefringence is induced when the local dielectric tensor becomes anisotropic due to the local orientational order of the anisotropic molecules.

The tensor order parameter $Q_{\alpha\beta}$ is related to the local dielectric tensor as[41)]

$$Q_{\alpha\beta} = \frac{3}{2}\frac{(\varepsilon_{\alpha\beta} - \bar{\varepsilon}\,\delta_{\alpha\beta})}{\Delta\varepsilon}, \tag{IV-20}$$

where $\varepsilon_{\alpha\beta}$ is the dielectric tensor, $\bar{\varepsilon}$ is the mean dielectric constant in the absence of external perturbations and $\Delta\varepsilon$ is the anisotropy in the dielectric constant if all molecules are perfectly aligned in one direction. We choose x to be the direction in which ultrasonic wave is propagating and z to be the direction of the optical beam whose polarization lies in the yz plane. The direction of the polarization is at 45° from the y axis.

Ultrasound propagating in the x direction induces a non-zero component of $Q_{\alpha\beta}$ and the resultant breakdown in the isotropy of the dielectric tensor causes the birefringence. The relation of $Q_{\alpha\beta}$ to the birefringence can be obtained as follows,

$$\begin{aligned}\Delta n &= \sqrt{\varepsilon_{xx}} - \sqrt{\varepsilon_{yy}} \\ &= \sqrt{\bar{\varepsilon} + 2\Delta\varepsilon Q_{xx}/3} - \sqrt{\bar{\varepsilon} + 2\Delta\varepsilon Q_{yy}/3}\ . \\ &\cong \frac{\Delta\varepsilon}{3\sqrt{\bar{\varepsilon}}}(Q_{xx} - Q_{yy})\end{aligned} \tag{IV-21}$$

As mentioned in the previous subsection, the relations $Q_{xx} + Q_{yy} + Q_{zz} = 0$ and $Q_{yy} = Q_{zz}$ hold. Therefore, Eq. (IV-21) can be written as,

$$\Delta n = \frac{\Delta\varepsilon}{2\bar{n}} Q_{xx}\ , \tag{IV-22}$$

where $\bar{n}$ is the mean refractive index which refers to the dielectric constant as $\bar{n} = \sqrt{\bar{\varepsilon}}$. We consider a plane wave propagating in the x direction: $Q_{xx} = \tilde{Q}_{xx} \exp[i(\omega t - qx)]$, $\delta\rho = \delta\tilde{\rho} \exp[i(\omega t - qx)]$, $v_x = \tilde{v}_x \exp[i(\omega t - kx)]$.
Equations for the density conservation and the relaxation of the order parameter are written as

$$i\omega\delta\tilde{\rho} - iq\rho\tilde{v}_x = 0 \tag{IV-23}$$

$$i\omega\tilde{Q}_{xx} + \Gamma\tilde{Q}_{xx} - iq\frac{4\mu}{3\nu}\tilde{v}_x = 0 \tag{IV-24}$$

Eliminating $\tilde{v}_x$ from Eqs. (IV-23) and (IV-24), the relation of $\delta\tilde{\rho}$ to $\tilde{Q}_{xx}$ is obtained as,

$$\tilde{Q}_{xx} = \frac{4}{3}\frac{\mu}{\nu}\frac{\delta\tilde{\rho}}{\rho}\frac{i\omega}{i\omega + \Gamma} \tag{IV-25}$$

Substituting the thermodynamic relation,

$$\delta\tilde{\rho} = (\partial\rho/\partial p)_s \delta\tilde{p} = c_0^{-2}\delta\tilde{p}\,, \tag{IV-26}$$

where $\delta\tilde{\rho}$ is the amplitude of the pressure perturbation, into Eq. (IV-25) and using the definition of the ultrasonic intensity, $W_U = \delta\tilde{p}^2/2\rho c_0$, the modulus of $\tilde{Q}_{xx}$ is obtained as,

$$\left|\tilde{Q}_{xx}\right| = \frac{4}{3}\frac{\mu}{A}\sqrt{\frac{2W_U}{\rho c_0^{\,3}}}\ \frac{\omega}{\sqrt{1 + (\omega/\Gamma)^2}}\ . \tag{IV-27}$$

The root mean square of the ultrasonically induced birefringence Δn_{rms} is acquired as,

$$\Delta n_{rms} = \frac{\Delta\varepsilon}{2\bar{n}} \cdot \frac{\left|Q_{xx}\right|}{\sqrt{2}} = \frac{2\Delta\varepsilon\mu}{3\bar{n}A}\sqrt{\frac{W_U}{\rho c_0^{\,3}}}\ \frac{\omega}{\sqrt{1 + (\omega/\Gamma)^2}}\ . \tag{IV-28}$$

The flow birefringence Δn_f under a constant shear strain rate G is obtained as Eq. (IV-39) in following flow birefringence section,

$$\Delta n_f = -2\mu G\Delta\varepsilon/(3\bar{n}A). \tag{IV-29}$$

Thus, the ultrasonically induced birefringence is related to the flow birefringence by,

$$\Delta n_{\mathrm{rms}} = \left| \frac{\Delta n_{\mathrm{f}}}{G} \right| \sqrt{\frac{W_{\mathrm{U}}}{\rho {c_0}^3}} \frac{\omega}{\sqrt{1 + (\omega/\Gamma)^2}} . \tag{IV-30}$$

Frenkel derived an expression for the ultrasonically induced birefringence similar to Eq. (IV-28).[51),52)] His treatment is very akin to ours in coupling the anisotropy tensor of the molecular orientation to the traceless part of the strain rate tensor. Our treatment, however, is based on a standard theory of irreversible thermodynamics and gives a concrete expression for the proportionality constant that appeares in his theory.

Peterlin derived the following expression for ultrasonically induced birefringence using the rotational diffusion equation for an ellipsoid under a longitudinal ultrasound;[52),53)]

$$\Delta n_{\mathrm{rms}}^{\mathrm{Peterlin}} = \bar{n} \left(\frac{\bar{n}^2 + 2}{3\bar{n}} \right)^2 \frac{4\pi}{5} N_0 (\alpha_1 - \alpha_2) \frac{\bar{\beta}}{6D} \sqrt{\frac{W_{\mathrm{U}}}{\rho {c_0}^3}} \frac{\omega}{\sqrt{1 + (\omega/6D)^2}} , \tag{IV-31}$$

where N_0 is the number density of the ellipsoid, α_1 and α_2 are the polarizability along and perpendicular to the principal axis of the ellipsoid, respectively and D is the rotational diffusion constant. $\bar{\beta}$ is a constant depending on the molecular shape and defined as, $\bar{\beta} = ({\alpha_1}^2 - {\alpha_2}^2)/({\alpha_1}^2 + {\alpha_2}^2)$, where α_1 and α_2 are the long and short diameters of the ellipsoid, respectively. Although the collective effect was not included in Peterlin's theory, the intensity and frequency dependence is the same as that in Eq. (IV-28), if the term $6D$ is replaced by Γ. The formula for flow birefringence is also obtained in the same framework as,[52),53)]

$$\left| \frac{\Delta n_{\mathrm{f}}}{G} \right|^{\mathrm{Peterlin}} = \bar{n} \left(\frac{\bar{n}^2 + 2}{3\bar{n}} \right)^2 \frac{4\pi}{5} N_0 (\alpha_1 - \alpha_2) \frac{\bar{\beta}}{6D} . \tag{IV-32}$$

Substituting Eq. (IV-32) into (IV-31), the following relation is obtained:

$$\Delta n_{\mathrm{rms}}^{\mathrm{Peterlin}} = \left| \frac{\Delta n_{\mathrm{f}}}{G} \right|^{\mathrm{Peterlin}} \sqrt{\frac{W_{\mathrm{U}}}{\rho {c_0}^3}} \frac{\omega}{\sqrt{1 + (\omega/6D)^2}} . \tag{IV-33}$$

This equation is the same form as Eq. (IV-30).

Martinoty and Bader obtained Eq. (IV-28) for the ultrasonic birefringence of isotropic phase of liquid crystals substituting Eq. (IV-39) in place of $|\Delta n_{\mathrm{f}}/G|^{\mathrm{Peterlin}}$ into (IV-33). Their indirect derivation of Eq. (IV-28) is confirmed here.[21)]

Expressions for flow[45)] and ultrasonically induced birefringence[48)] were obtained by Kivelson and coworkers based on an irreversible statistical treatment as,

$$\left| \frac{\Delta n_{\mathrm{f}}}{G} \right|^{\mathrm{Kivelson}} = \frac{1}{\bar{n}} \left(\nu_{\mathrm{K}} \cdot \frac{R_{\mathrm{Total}} \Delta_\mu}{1 + \Delta_\mu} \cdot \frac{\eta_{\mathrm{S}}}{k_{\mathrm{B}} T} \cdot \frac{R}{\Gamma} \right)^{1/2} \frac{{\lambda_0}^2}{\pi} \tag{IV-34}$$

$$\Delta n_{\mathrm{rms}}^{\mathrm{Kivelson}} = \frac{1}{2\bar{n}} \left(\nu_{\mathrm{K}} \cdot \frac{R_{\mathrm{Total}} \Delta_\mu}{1 + \Delta_\mu} \cdot \frac{\eta_{\mathrm{S}}}{k_{\mathrm{B}} T} \cdot \frac{R}{\Gamma} \right)^{1/2} \frac{{\lambda_0}^2}{\pi} \sqrt{\frac{W_{\mathrm{U}}}{\rho {c_0}^3}} \frac{\omega}{\sqrt{1 + (\omega/\Gamma)^2}} \tag{IV-35}$$

where R_{Total} is the total light scattering per unit volume, Δ_μ is the depolarization ratio, ν_K is the ratio of the central Lorenztian HH Rayleigh line relative to the total depolarized light scattering intensity, k_B is the Boltzmann constant, T is the temperature and R is the coupling parameter of the molecular reorientation to the translational motion. It should be noted, however, the proportionality constant in Eqs. (IV-30) and (IV-33) differs by a factor of 2 from that implied by Eqs. (IV-34) and (IV-35).

3) Flow Birefringence

The formula for flow birefringence has been already obtained.[3),43),44)] For ease of comprehension, we will here mention its derivation.

Consider a stationary shear strain rate G in which fluid flows in the x direction with its gradient parallel to the y axis. Taking into account the stationary condition, Eqs. (IV-13) and (IV-14) relate the order parameter to the strain rate as,

$$-AQ_{xy} = -AQ_{yx} = \mu G \tag{IV-36}$$

The dielectric tensor is then written as,

$$\begin{pmatrix} \bar{\varepsilon} & \delta\varepsilon & 0 \\ \delta\varepsilon & \bar{\varepsilon} & 0 \\ 0 & 0 & \bar{\varepsilon} \end{pmatrix}, \tag{IV-37}$$

where $\delta\varepsilon$ is defined as $\delta\varepsilon = -2\mu G\Delta\varepsilon/3A$. By choosing new axes XY, which are rotated counterclockwise from the xy axes by 45°, the dielectric tensor can be written as,

$$\begin{pmatrix} \bar{\varepsilon} + \delta\varepsilon & 0 & 0 \\ 0 & \bar{\varepsilon} - \delta\varepsilon & 0 \\ 0 & 0 & \bar{\varepsilon} \end{pmatrix}. \tag{IV-38}$$

The birefringence Δn_f is then obtained from

$$\begin{aligned} \Delta n_f &= \sqrt{\varepsilon_{XX}} - \sqrt{\varepsilon_{YY}} \\ &= \sqrt{\bar{\varepsilon} + \delta\varepsilon} - \sqrt{\bar{\varepsilon} - \delta\varepsilon}\ . \\ &\cong \frac{\delta\varepsilon}{\sqrt{\bar{\varepsilon}}} = -\frac{2\mu G\Delta\varepsilon}{3\bar{n}A} \end{aligned} \tag{IV-39}$$

APPENDIX: COMPARISION BETWEEN IRREVERSIBLE STATISTICAL TREATMENT AND DE GENNES' PHENOMENOLOGICAL ONE

From Eqs. (IV-15) to (IV-17), we can obtain the dispersion relation of the sound waves as,

$$-i\omega^3-\omega^2\left(\frac{q^2}{\rho}\left(\eta_V+\frac{4}{3}\eta_S\left(1-\frac{2\mu^2}{\eta_V\nu}\right)\right)+\Gamma\right)+$$
$$i\omega\left(\frac{q^2}{\rho}\left(\eta_V+\frac{4}{3}\eta_S\right)\Gamma+{c_0}^2q^2\right)+{c_0}^2q^2\ \Gamma=0 \qquad \text{(IV-A1)}$$

Alms *et al.*[27] compared the irreversible statistical treatment on the reorientational-translational coupling with de Genne's phenomenological one for the purely shear case. They derived the relationship of the coupling parameter "*R*" between reorientational and transverse translational modes to the phenomenological transport coefficients μ and ν as,

$$R=\frac{2\mu^2}{\eta_S\nu}. \qquad \text{(IV-A2)}$$

Although the coupling of the longitudinal translation to the reorientational mode is considered in this paper, Eq. (IV-A2) is valid in our case for the following reason. In our approach, the longitudinal velocity gradient and its conjugated stress are divided into isotropic and anisotropic terms and only the latter terms are coupled to the tensor order parameter and its conjugated stress variable, as introduced by de Gennes. The definition of the parameters μ and ν is the same as that for the purely shear case.

Equation (IV-A1) can be expressed as follows,

$$\frac{\omega^2}{q^2}={c_0}^2+i\omega\frac{1}{\rho}\left(\eta_V+\frac{4}{3}\eta_S\left(1-R\frac{i\omega}{i\omega+\Gamma}\right)\right). \qquad \text{(IV-A3)}$$

If the coupling parameter *R* is zero, Eq. (IV-A3) reduces to the ordinary dispersion relation of sound waves. It should also be noted that in the case of simple shear, de Gennes derived an effective dynamic shear viscosity $\eta_S^*(\omega)$,[3),43)]

$$\eta_S^*(\omega)=\eta_S\left(1-R\frac{i(\omega/\Gamma)}{1+i(\omega/\Gamma)}\right). \qquad \text{(IV-A4)}$$

If Eq. (IV-A4) is substituted in place of the shear viscosity η_S in the ordinary dispersion relation, the Eq. (IV-A3) is obtained again. In the limit Im(k)/Re(k) << 1, we obtain from Eq. (IV-A3) approximate expressions for the sound velocity dispersion and absorption coefficient:

$$c=c_0\left(1+\frac{2}{3\rho{c_0}^2}\eta_SR\frac{\omega^2\Gamma}{\omega^2+\Gamma^2}\right), \qquad \text{(IV-A5)}$$

$$\alpha=\frac{\omega^2}{2{c_0}^3\rho}\left(\eta_V+\frac{4}{3}\eta_S(1-R)+\frac{4}{3}\eta_SR\frac{\Gamma^2}{\omega^2+\Gamma^2}\right). \qquad \text{(IV-A6)}$$

In the low frequency limit, Eq. (IV-A5) reduces to $c = c_0$, and Eq. (IV-A6) becomes the ordinary classical sound absorption:

$$\alpha = \frac{\omega^2}{2 {c_0}^3 \rho} \left(\eta_V + \frac{4}{3} \eta_S \right) \tag{IV-A7}$$

Grubbs and MacPhail have derived the VV light scattering density function from the following equations,[49)]

$$\dot{D}_{xx-yy} = -\Gamma D_{xx-yy} - i\Gamma (\alpha R)^{1/2} p_x \tag{IV-A8}$$

$$\dot{D}_{zz} = -\Gamma D_{zz} - i\Gamma (\alpha R/3)^{1/2} p_x \tag{IV-A9}$$

$$\dot{n} = i c_0 q p_x \tag{IV-A10}$$

$$\begin{aligned} \dot{p}_x = &- i\Gamma (\alpha R)^{1/2} D_{xx-yy} - i\Gamma (\alpha R/3)^{1/2} D_{zz} - i c_0 q n \\ &- \Gamma \alpha [\eta_V / \eta_S + (1-R) 4/3] p_x \end{aligned} \tag{IV-A11}$$

where $D_{xx-yy}(q, t)$ and $D_{zz}(q, t)$ are the orientational density tensor components, $n(q, t)$ is the number density, $p_x(q, t)$ is the longitudinal momentum density, and $\alpha = q^2 \eta_S / \rho\Gamma$. Unlike in the original theory of Lipeles and Kivelson,[48)] the coupling to $D_{zz}(k, t)$ term is considered. Using Fourier transforms, the dispersion relation is obtained from Eqs. (IV-A8) to (IV-A11) as,

$$\begin{aligned} (i\omega + \Gamma) \Bigg[&- i\omega^3 - \omega^2 \left(\frac{q^2}{\rho} \left(\eta_V + \frac{4}{3} \eta_S (1-R) \right) + \Gamma \right) \\ &+ i\omega \left(\frac{q^2}{\rho} \left(\eta_V + \frac{4}{3} \eta_S \right) \Gamma + {c_0}^2 q^2 \right) + {c_0}^2 q^2 \Gamma \Bigg] = 0 \end{aligned} \tag{IV-A12}$$

The term in the second parenthesis is identical to the left hand of the Eq. (IV-A1). The relation $i\omega + \Gamma = 0$ represents the non-propagating mode, thus the expressions for the sound velocity and absorption are identical to Eqs. (IV-A5) and (IV-A6) respectively. The sound velocity and absorption relations which appeared in the Lipeles and Kivelson paper are not identical to those obtained here since the coupling to $D_{zz}(q, t)$ term is not taken into account in their paper.[48)] However, the Lipeles-Kivelson expression for ultrasonically induced birefringence still remains as in Eq. (IV-35), since only Eqs. (IV-A8) and (IV-A10) are necessary to derive the expression of ultrasonically induced birefringence.

Since Eqs. (IV-A9) to (IV-A12) are not equivalent to Eqs. (IV-15) to (IV-19), the spectral density functions for the VV light scattering obtained from our transport equations are different from those obtained by Grubbs and MacPhail. For example, the spectral density of Q_{zz},

$$J_{QQ}(q, \omega) = \mathrm{Re} \int_0^\infty dt \exp(i\omega t) \left\langle Q_{zz}(q, t) Q_{zz}^*(q, 0) \right\rangle \Big/ \left\langle \left| Q_{zz}(q, 0) \right|^2 \right\rangle , \tag{IV-A13}$$

is approximately obtained using the Laplace-Fourier transform[1)] when $c_0 k >> \eta_V q^2/\rho$, $\eta_S q^2/\rho$ as,

$$J_{QQ}(k, \omega) = \left(1 + \frac{4}{3}\eta_S \frac{q^2}{\rho} \Gamma R \frac{\Gamma^2 - {c_0}^2 q^2}{(\Gamma^2 + {c_0}^2 q^2)^2}\right) \frac{\Gamma_R}{\omega^2 + \Gamma_R^2}$$
$$- \frac{2}{3}\eta_S \frac{q^2}{\rho} \Gamma \frac{\Gamma^2 - {c_0}^2 q^2}{(\Gamma^2 + {c_0}^2 q^2)^2} \left(\frac{\Gamma_B}{(\omega - \omega_B)^2 + \Gamma_B^2} + \frac{\Gamma_B}{(\omega + \omega_B)^2 + \Gamma_B^2}\right), \quad \text{(IV-A14)}$$
$$- \frac{4}{3}\eta_S \frac{q^2}{\rho} \Gamma \frac{c_0 q \Gamma}{(\Gamma^2 + c_0 q^2)^2} \left(\frac{\omega_B - \omega}{(\omega - \omega_B)^2 + \Gamma_B^2} + \frac{\omega_B + \omega}{(\omega + \omega_B)^2 + \Gamma_B^2}\right)$$

where Γ_R, ω_B and Γ_B are given by the equations,

$$\Gamma_R = \Gamma - \frac{4}{3}\frac{q^2}{\rho}\eta_S R \frac{\Gamma^2}{\Gamma^2 + {c_0}^2 q^2}, \quad \text{(IV-A15)}$$

$$\omega_B = c_0 q \left(1 + \frac{2}{3}\frac{q^2}{\rho}\eta_S R \frac{\Gamma}{\Gamma^2 + {c_0}^2 q^2}\right), \quad \text{(IV-A16)}$$

$$\Gamma_B = \frac{1}{2}\left(\frac{q^2}{\rho}\left(\eta_V + \frac{4}{3}\eta_S\left(1 - R\frac{{c_0}^2 q^2}{\Gamma^2 + {c_0}^2 q^2}\right)\right)\right). \quad \text{(IV-A17)}$$

Equation (IV-A14) is different from Eq. (8b) of Ref. 49. Wang derived the spectral density of the density fluctuation $\delta\rho$ as,[50)]

$$J_{\rho\rho}(q, \omega) = \mathrm{Re}\int_0^\infty dt \exp(i\omega t) \left\langle \delta\rho(q, t)\, \delta\rho_{zz}^*(q, 0)\right\rangle \Big/ \left\langle \left|\delta\rho(q, 0)\right|^2 \right\rangle$$
$$= \mathrm{Re}\left(\frac{i\omega + \frac{q^2}{\rho}\left(\eta_V + \frac{4}{3}\eta_S\left(1 - R\frac{i\omega}{i\omega + \Gamma}\right)\right)}{{c_0}^2 q^2 + i\omega\left(i\omega + \frac{q^2}{\rho}\left(\eta_V + \frac{4}{3}\eta_S\left(1 - R\frac{i\omega}{i\omega + \Gamma}\right)\right)\right)}\right) \quad \text{(IV-A18)}$$

The same results can be obtained from Eqs. (IV-15) to (IV-19). Eq. (IV-A18) is not identical with Eq. (8a) of Ref. 49. The differences demonstrated above come from the difference in the choice of the coupled variables. In the statistical approach, the reorientational densities D_{xx-yy} and D_{zz} were chosen and were directly coupled to the longitudinal momentum density. On the other hand, in our

treatment, the translational term was divided into isotropic and anisotropic components and the only latter couples to the reorientational mode.

V. Ultrasonically Induced Birefringence in Liquids and Solutions

1. Introduction

The birefringence is induced in liquids and solutions containing certain amount of nonspherical particles as a result of the particle orientation due to ultrasonic waves. This was called the phenomenon of the ultrasonically induced birefringence.[54] The early theoretical studies of the birefringence have been reviewed by Hilyard and Jerrard.[52] The theory developed by Oka[55] indicated that large disc-like rigid particles align by hydrodynamics torque which is produced by the radiation pressure due to the passage of the ultrasonic waves. The normal of disclike particles is parallel to the ultrasonic field, and the sign of the birefringence of disk particles is negative. The measurements of the birefringence of large rigid disc-like particles were carried out on bentonite[56] and gold sols.[12),57] These experimental results show that the birefringence is proportional to the ultrasonic intensity as predicted by the Oka theory. Ou-Yang *et al.*[15] made use of the Raman-Nath diffraction effect to measure the ultrasonic intensity at the frequency range from 1 to 19 MHz and investigated the ultrasonically induced birefringence of gold sols as a function of solvent viscosity, particle size and ultrasonic intensity and frequency. The birefringence increased with increasing ultrasonic frequency and decreasing viscosity and the sign of the birefringence was positive. They modified the Oka theory to explain the sign of the birefringence and the dependence of the birefringence on the frequency and viscosity.

For large rigid rod-like particles, no theoretical study of the ultrasonically induced birefringence has been reported. Experimental investigations on the birefringence of V_2O_5 sols[39),54),56] have been carried out so far. The ultrasonically induced birefringence of V_2O_5 sols was proportional to the ultrasonic intensity and the volume fraction as predicted by the Oka theory.[39] Petralia also indicated that the birefringence depends on the viscosity and the sign of the birefringence is positive.[56] No experimental investigation of the frequency dependence of the birefringence of rod-like rigid particles has been carried out.

On the contrary, for neat liquids, a sinusoidal velocity gradient can directly produce sinusoidal orientational order. The reorientational order produced is not uniform but propagates as waves and the induced birefringence should be proportional to the ultrasonic amplitude, that is, the square root of the ultrasonic intensity.[15),42),54),56]

After the brief description of the modified Oka theory of ultrasonically induced birefringence for rod-like particles, we discuss the ultrasonically induced birefringence of liquid crystal in isotropic phase by comparing the experimental results with the expression obtained in the frame of the de Gennes's phenomenological theory.

Next, we would like to discuss the frequency dependence of the ultrasonically induced birefringence of rod-like particles. Birefringence for unit ultrasonic intensity has been estimated. The experimental results will be discussed on the basis of the modified Oka theory for rod-like particles. In addition, orientational relaxation times of rod-like particles have also been evaluated from the trace of the transient birefringence.

Finally, we would like to describe our recent results for ultrasonically induced birefringence of the rodlike micelles in the aqueous salt solutions and polymer solutions.

2. Modified Oka Theory for Rodlike Particles[20)]

Application of ultrasonic fields will induce the birefringence Δn, which is given by

$$\Delta n = 2\pi \Delta G \Theta \phi / n_0 \tag{V-1}$$

where Θ is the mean orientation of the particles, ΔG is the optical anisotropy, ϕ is the volume fraction of particles and n_0 is the refractive index of solvent. The mean orientation can be calculated from the distribution function of particles which is obtained by considering the potential energy due to the torque caused by the applied field.[58),59)] Oka[55)] assumed that the passage of acoustic waves sets up the radiation pressure so that large rigid disc-like particles are subject to the turning torque that will align them. The ultrasonic torque is estimated by considering the Rayleigh disc[60),61)] problem. At this point we extend the modified Oka theory for disc-like particles in view of application to prolate particles. We assumed that prolate particles such as α-Fe_2O_3 sols and PTFE latex are also subject to the torque due to radiation pressure. König[62)] derived the time averaged torque $|M|$ for prolate particles as

$$\left| M \right| = X \rho_0 \, a \, b^2 \quad (v-u)^2 \sin 2\theta \tag{V-2}$$

$$X = \frac{2\pi\varepsilon^3 \left[\dfrac{2\varepsilon^3}{3} + \dfrac{1}{2}(1-\varepsilon^2) \ln\left[\dfrac{1+\varepsilon}{1-\varepsilon}\right] - \varepsilon \right]}{\left[\dfrac{1}{2}(1-\varepsilon^2) \ln\left[\dfrac{1+\varepsilon}{1-\varepsilon}\right] - \varepsilon \right] \left[2\varepsilon^3 + \dfrac{1}{2}(1-\varepsilon^2) \ln\left[\dfrac{1+\varepsilon}{1-\varepsilon}\right] - \varepsilon \right]} \tag{V-3}$$

with $\varepsilon = (a^2 - b^2)^{1/2}/a$, where v the fluid velocity, u is the translational velocity of particle, a and b are the radii of major and minor axes of the particle, respectively, ρ_0 is the densities of solvent and θ is an angle between the major axis of prolate spheroids and the direction of ultrasonic propagation. If the ultrasonic energy is small compared with the thermal disturbance, the birefringence is expressed as

$$\Delta n = \frac{4X\pi \, a \, b^2 \Delta G \phi \, A^2 F^2}{15 k_B T V_S^{\,0} n_s} \tag{V-4}$$

where $V_S^{\,0}$ the sound velocity of solvent, A is the ultrasonic amplitude, k_B is the Boltzmann constant, and T is the temperature. For spheroid particles, ΔG is obtained by an extension of the theory of Peterlin and Stuart[63)] as

$$\Delta G = \frac{n_0^2 \left(n^2 - n_0^2 \right)^2 (N_2 - N_1)}{\left[4\pi n_0^2 + (n^2 - n_0^2) N_1 \right] \left[4\pi n_0^2 + (n^2 - n_0^2) N_2 \right]} \tag{V-5}$$

where n is the refractive index of particles, respectively and for prolate particles N_1 and N_2 are shape factors along a and b, respectively. The N_1 and N_2 are obtained by

$$N_1 = 2\pi(\mu^2 - 1)\left(\mu \ln \frac{\mu+1}{\mu-1} - 2\right), \quad N_2 = N_3 = \frac{4\pi - N_1}{2} \tag{V-6}$$

with $\mu = a/(a^2 - b^2)^{1/2}$.

Ou-Yang *et al.*[15] indicated that the suspended particles which execute translational oscillations in fluid are subject to the drag force that is shown in terms of the librational Reynolds number $R_L = a^2\omega\rho_0/2\eta_S$, where ω is the ultrasonic angular frequency and η_S is the shear viscosity of the solvent.[64] They supposed that the translational motion is much faster than the orientational motion and the equation of translational motion for particles in dilute region is expressed as

$$F = \frac{v-u}{v} = \frac{\rho - \rho_0}{\rho + i(\varsigma / V\omega)\left[\left(1 + \sqrt{R_L}\right) - i\left(\sqrt{R_L} + \gamma R_L\right)\right]} \tag{V-7}$$

where V is the particle volume, ζ is the Stokes' drag coefficient and γ is a constant. When the prolate particles are translating in the direction normal to its major axis, the ζ is given[65] as

$$\zeta = \frac{16\pi\eta_S\, a b^2}{(\chi + a^2\alpha)} \tag{V-8}$$

where

$$\alpha = a b^2 \int_0^\infty \frac{dx}{\sqrt{a^2 + x}\left(b^2 + x\right)^2} \tag{V-9}$$

and

$$\chi = a b^2 \int_0^\infty \frac{dx}{(b^2 + x)\sqrt{a^2 + x}} \tag{V-10}$$

If $R_L = \infty$, the parameter F in viscous fluids is reduced to that in ideal fluid. For ideal fluid, F is obtained from the inertia-coefficient of a prolate particle.

$$F = \frac{\rho - \rho_0}{\rho + \dfrac{\alpha}{2-\alpha}\rho_0}. \tag{V-11}$$

Comparing Eq. (V-7) with Eq. (V-12) lead to γ given as follows.

$$\gamma = \frac{\alpha(\chi - b^2\alpha)}{6\,a^2\,(2-\alpha)} \tag{V-12}$$

The frequency dependence of the birefringence of prolate, namely, rod-like particles can be expressed in terms of F which is obtained by substituting Eqs. (V-8), (V-10) and (V-12) into Eq. (V-7).

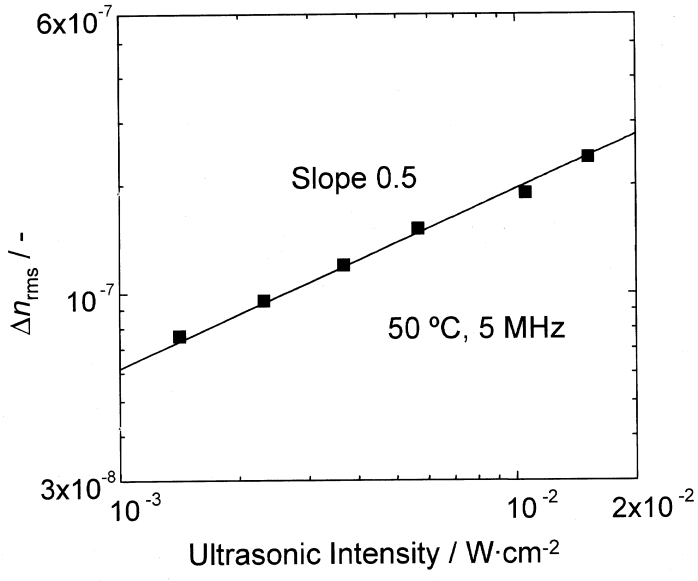

Fig. V-1 Ultrasonic intensity dependence of the root mean square of the induced birefringence of 5CB (Closed square) at 50°C. The solid line indicates the slope of 0.5.

3. Ultrasonically Induced Birefringence in Isotropic Phase in Neat Liquid Crystal[21)]

As shown in the preceding section, the theoretical expressions for the ultrasonically induced birefringence of liquids and solutions are obtained in the frame of the de Gennes' phenomenological theory.

The isotropic phase of liquid crystals is most appropriate to examine the expression obtained, because the relaxation frequencies of the orientational motions are in the same order of ultrasonic frequencies usually used.[17)] Besides, the flow birefringence for isotropic phase of liquid crystals, *p*-*n*-pentyl *p*'-cyanobiphenyl (5CB), has been already reported by Martinoty *et al.*[42)] The values of the flow birefringence and the relaxation frequencies are required for the reproduction of the frequency dependence of the ultrasonically induced birefringence.

To confirm our expression quantitatively, we measured the ultrasonically induced birefringence of *p*-*n*-pentyl *p*'-cyanobiphenyl (5CB) in the isotropic phase as a function of frequency (frequencies at 3,5,7,11, and 13 MHz) at temperature of 50 and 55°C.

Figure V-1 shows the ultrasonic intensity dependence of the birefringence in 5CB at 50°C. The slope of the solid line for this logarithmic plot is 0.5, indicating the birefringence is proportional to the square root of the ultrasonic intensity. This result is in good agreement with Eq. (IV-30).

$$\Delta n_{\mathrm{rms}} = \left| \frac{\Delta n_{\mathrm{f}}}{G} \right| \sqrt{\frac{W_{\mathrm{U}}}{\rho {c_0}^3}} \frac{\omega}{\sqrt{1 + (\omega/\Gamma)^2}} . \qquad \text{(IV-30)}$$

Figure V-2 shows frequency dependence of $\Delta n_{\mathrm{rms}} {W_{\mathrm{U}}}^{-1/2}$. The value of $\Delta n_{\mathrm{rms}} {W_{\mathrm{U}}}^{-1/2}$ increases but the slope $\partial(\Delta n_{\mathrm{rms}} {W_{\mathrm{U}}}^{-1/2})/\partial f$ decreases with increasing frequency. The solid curves in Fig. V-2 are the calculated ones obtained by substituting into Eq. (IV-30) the values of $|\Delta n_{\mathrm{f}}/G|$ from flow birefrin-

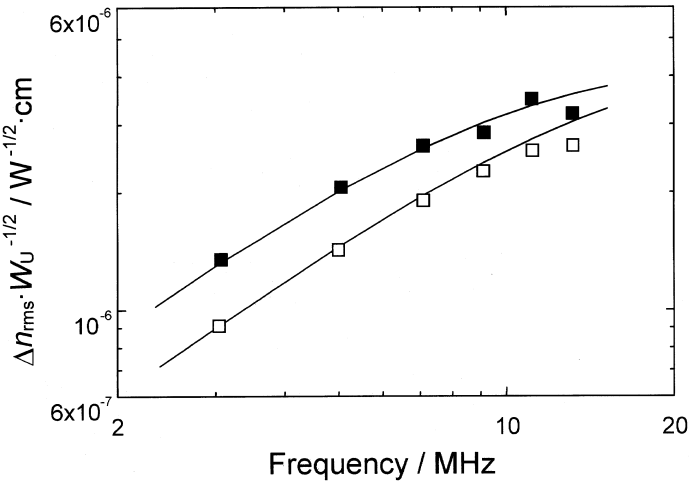

Fig. V-2 Frequency dependence the birefringence per the square root of the ultrasonic intensity at 50 (closed) and 55 (open) °C. Solid curves indicate the estimation from Eq. (IV-30). The detailed explanations are given in the text.

gence measurements[42] and Γ from optical beating light scattering experiments.[17] The values of $|\Delta n_f/G|$ are 1.86 and 1.26 ns and those of $\Gamma/2\pi$ are 10.0 and 15.3 MHz at 50 and 55°C, respectively. The observed values of $\Delta n_{rms} W_U^{-1/2}$ in this study are satisfactorily reproduced by Eq. (IV-30).

Martinoty and Bader measured the ultrasonically induced birefringence for the isotropic phase of liquid crystals.[41),42] In their experiment, however, only the relative values of the ultrasonic intensity were measured and they examined Eq. (IV-30) in terms of the temperature dependence of the birefringence at three different frequencies. In this work, we directly measured the ultrasonically induced birefringence as a function of frequency and ultrasonic intensity. Our results are reproduced completely by the equation derived here. Moreover, the absolute values of ultrasonically induced birefringence obtained in this work are in good agreement with those calculated using the flow birefringence and reorientational relaxation frequency obtained by light scattering. This indicates clearly that our theoretical treatment is valid and the method of ultrasonic intensity measurement presented here is very useful.

4. Frequency Dependence of Ultrasonically Induced Birefringence of Rod-like Particles[20]

1) Introduction

For large rigid rod-like particles, no theoretical study of the ultrasonically induced birefringence has been reported. Experimental investigations on the birefringence of V_2O_5 sols[39),54),56] have been carried out so far. Measurements[56] by Petralia on V_2O_5 sols indicated that the birefringence depended on the viscosity and the sign of the birefringence was positive. In our previous paper,[39] the ultrasonically induced birefringence of V_2O_5 sols was proportional to the ultrasonic intensity and the volume fraction, as predicted by the Oka theory. However, no experimental investigation of the frequency dependence of the birefringence of rod-like rigid particles has been carried out. Furthermore, the mean axis ratio of V_2O_5 used was 1/70 and at the volume concentration $1.28 - 6.40 \times 10^{-4}$, the distance of the center of gravity of the rodlike particles of 1.7 μm long was 1.1 –

1.8 μm and almost same order of the length of the particle. This means that the V_2O_5 sol is not in dilute, but in semi-dilute regions.

In order to elucidate the frequency dependence of the ultrasonically induced birefringence and the orientational relaxation time of rod-like particles, we used the hematite (α-Fe_2O; axial ratio = 5.5, the volume fraction was varied from 9.4×10^{-8} to 2.4×10^{-5}) sol of rodlike particles and poly (tetrafluoroethylene) (PTFE; the average length of major axis of 0.55 μm and the average axial ratio of 1.9. The volume fraction was varied from 1.3×10^{-7} to 8.2×10^{-4}.) latex of prolate particles.

2) Birefringence of Rod-like Particles

The Oka theory[55] indicates that the birefringence is proportional to the ultrasonic intensity and volume fraction. In his theory, the solvent is assumed to be as ideal fluid and the birefringence does not depend on the ultrasonic frequency nor the solvent viscosity. As shown in the Figs. V-3 and V-4, the birefringence of α-Fe_2O_3 and PTFE particles is proportional to the ultrasonic intensity and volume fraction and depends on the frequency and viscosity. This means that the birefringence of rod-like particles is not fully interpreted by the Oka theory.

Ou-Yang *et al.*[15] modified the Oka theory to explain the frequency and viscosity dependence of the birefringence of conducting disc-like gold sols. We have extended the modified Oka theory for disc-like particles in view of application for rod-like particles. The birefringence of rod-like particles is given by:

$$\Delta n = \frac{4X\pi a b^2 \Delta G \phi A^2 F^2}{15 k_B T V_S^{\,0} n_s} \qquad \text{(V-4)}$$

where ΔG is the optical anisotropy, ϕ the volume fraction, $V_S^{\,0}$ the sound velocity of solvent. The F is given as

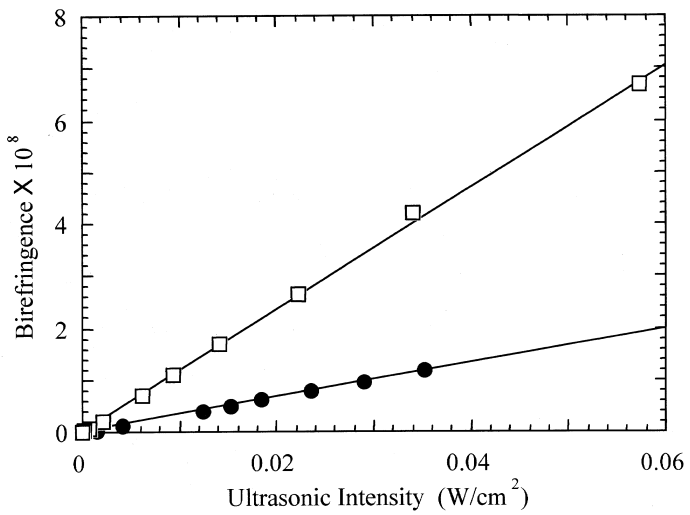

Fig. V-3 Birefringence against ultrasonic intensity at 25°C (25 MHz): (●) α-Fe_2O_3 sols at volume fraction 4.7×10^{-6}; (□) PTFE latex at volume fraction 7.6×10^{-5}.

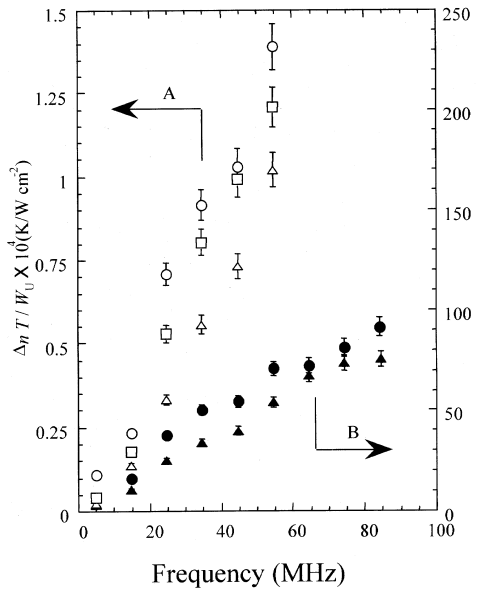

Fig. V-4 Plots of $\Delta n\, T/W_U$ against the ultrasonic frequency.
A. α-Fe_2O_3 sols of (volume fraction = 4.7×10^{-6}). Temperature: (○) 50°C; (□) 25°C; (△) 10°C.
B. PTFE latex (volume fraction = 8.2×10^{-4}). Temperature: (●) 50°C; (▲) 10°C.

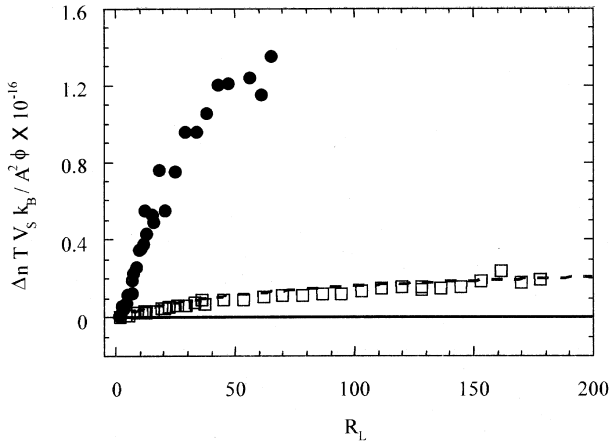

Fig. V-5 Plots of normalized birefringence $\Delta n\, TV_S k_B/A^2\phi$ against R_L: (●) α-Fe_2O_3 sols; (□) PTFE latex; Dotted (Fe_2O_3 sols) and solid (PTFE latex) curves show the theoretical values.

$$F = \frac{v-u}{v} = \frac{\rho - \rho_0}{\rho + i(\zeta / V\omega)\left[\left(1+\sqrt{R_L}\right) - i\left(\sqrt{R_L} + \gamma R_L\right)\right]} \qquad \text{(V-7)}$$

with $R_L = a^2\omega\rho_0/2\eta$ where ρ and ρ_0 are the densities of particles and solvent, respectively, v the fluid velocity, u the translational velocity of particle, ζ the Stokes' drag coefficient, ω the ultrasonic angular frequency, V the particle volume and γ a constant. The reduced birefringence $\Delta n T V_S k_B/A^2\phi$ can be estimated from the results in Figs. V-3 and V-4. The results are shown in Fig. V-5, where the theoretical line is included. For α-Fe_2O_3 sols, the experimental values are about 20 times larger than the theoretical values and for PTFE latex, while the experimental values are about 100 times as large as the theoretical values. The large deviations from the theoretical values can not be explained in terms of the modified Oka theory for rod-like particles, even if one takes into account the experimental and estimation errors in the refractive index and the size of the particle.

In the Oka theory, the turning torque which aligns the disc-like particles was derived from the Euler equation for ideal fluid and the ultrasonically induced birefringence was predicted to be proportional to F^2, namely, $[(v\text{-}u)/v]^2$. The value of F in ideal fluid does not depend on the frequency and viscosity. Ou-Yang *et al.*[15] modified the Oka theory to interpret the frequency dependence of the birefringence of disc-like particles in viscous fluids. In the modified Oka theory, the parameter F in the Oka theory was replaced by the one derived from the Navier-Stokes equation for viscous fluids. However, the turning torque also should be modified on the basis of the Navier-Stokes equation. In addition, under oscillatory motion, the flow around the rod-like particles is complicated and the flow may be in eddy or stagnation. A new theory of the ultrasonically induced birefringence should be required for the case of rod-like particles after taking into account of turning torque

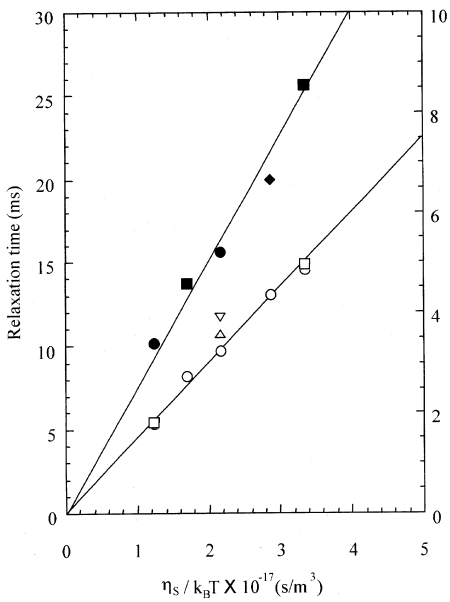

Fig. V-6 Orientational relaxation time for α-Fe_2O_3 sols and PTFE latex against η_S/k_BT. A. α-Fe_2O_3 sols (volume fraction: (□) 2.4×10^{-5}; (○) 4.7×10^{-6}). B. PTFE latex (volume fraction: (■) 4.1×10^{-3}; (●) 7.6×10^{-5}; (◆) 2.6×10^{-6}. The orientational relaxation times for α-Fe_2O_3 sols obtained by transient magnetic birefringence[68] measurements are also included. Field strength: (△) high; (▽) low.

in viscous fluids and the boundary condition of fluids around the rod-like particles.

3) Orientational Relaxation Times of Rod-like Particles

The birefringence decays after ultrasonic field disappears as shown in Experimental section (see Fig. II-4). This decay reflects the orientational relaxation process of the particles. The orientational relaxation time of the particles is obtained by fitting the extinction process of the birefringence to Eq. (II-9). The orientational relaxation times of α-Fe_2O_3 sols and PTFE latex are plotted against η_S/k_BT in Fig. V-6, where η_S is the solvent viscosity, T the temperature and k_B the Boltzmann constant. The figure demonstrates that the orientational relaxation time is proportional to η_S/k_BT. The orientational relaxation time τ of α-Fe_2O_3 and PTFE particles in dilute solution follows the Debye-Einstein equation,

$$\tau = \frac{\eta_S V^*}{k_B T} \tag{V-13}$$

where V^* is the effective volume of a particle. The effective volume of α-Fe_2O_3 and PTFE particle estimated from the slopes in Fig. V-6 are 1.5×10^{-20} and 7.6×10^{-20} m^3, respectively. According to Perrin,[66] V^* of a prolate particle is given as

$$V^* = \frac{8\pi a^3}{9}\left(\frac{1-p^4}{(2-p^2)\,G(p)-1}\right) \tag{V-14}$$

$$G(p) = \frac{1}{\left(1-p^2\right)^{1/2}} \ln\left[\frac{1+\left(1-p^2\right)^{1/2}}{p}\right] \tag{V-15}$$

where p is the axial ratio b/a and the a and b are the radii of major and minor axes of the particle, respectively. For PTFE latex, $2a$ calculated from Eqs. 2 and 3 is 0.80 μm with p = 1/1.9. The size of PTFE particles obtained from the electron microscopy is within 0.4 to 1.0 μm with an average value of 0.55 μm and it is smaller than the size estimated from the birefringence measurements. For α-Fe_2O_3 particles, the value of $2a$ is 0.55 μm with p = 1/5.5 and is consistent with the value reported by Ozaki.[67]

The extinction of the transient ultrasonically induced birefringence reflects the orientational relaxation process. Birefringence induced by magnetic and electric fields also involves the same information as the ultrasonically induced birefringence. James[68] estimated the orientational relaxation time of a-Fe_2O_3 sols from the measurements of the transient magnetic birefringence. He used the a-Fe_2O_3 sols with the average length of major axis 0.54 mm and the axial ratio ca. 5, while are nearly equal to those used in this work. Although, as is shown in Fig. V-6, the relaxation time obtained from the magnetic birefringence depends on the magnetic intensity, the values are close to those from the ultrasonically induced birefringence within the experimental error. James explained the intensity dependence of the relaxation time as follows. The larger particles are preferentially oriented in the low magnetic fields, while under the high magnetic fields all the particles are oriented. In the ultrasonically induced birefringence, the relaxation time is independent of the ultrasonic intensity investigated here. Irrespective of their size, the particles can be orientated by the radiation pressure.

As is shown in Fig. V-6, the orientational relaxation times of both α-Fe_2O_3 and PTFE particles can be expressed by the Debye-Einstein equation. This fact means that the orientational mo-

tion of these particles is not affected by the interparticle interaction. In other words, information of the orientational motion of isolated particles with large anisotropy is obtained by the ultrasonically induced birefringence, since the measurements in very dilute solution can be carried out.

5. Ultrasonically Induced Birefringence of Rodlike Micelles in Entanglement Networks[40)]

1) Introduction

Some surfactant molecules form rodlike micelles in aqueous solution.[69),70)] In the dilute concentration range, the solutions of these surfactants behave like sol.[71)] At higher concentrations, the rodlike micelles form the entanglement networks and the solutions show the pronounced viscoelasticity. The rodlike micelles are anisotropic aggregates and the solutions become birefringent by application of external fields. The dynamics of the entanglement networks of the rodlike micelles has been investigated by birefringence measurements such as electric birefringence[72)] and flow birefringence.[73)-75)] The results of studies showed some anomalous behaviors characteristic of the entanglement networks.

Hoffmann *et al.*[72)] investigated the rodlike micelles of hexadecyloctyldimethylammonium bromide by the electric birefringence. They indicated that the four different relaxation processes appear with changing the micelle concentrations. In the dilute range, a birefringence was observed with a first relaxation time which results from the orientation of the individual rods whose relaxation time is about 10^{-6} s. The length of rodlike micelle estimated from the first relaxation time agreed with the one determined by light scattering.[69)] The overlaping of the rodlike micelles gives rise to a second relaxation process having the relaxation time of about 10 times longer than that of the first process. In the concentrated region where the rodlike micelles form the network, third and fourth processes appears in the ranges from 1 ms to 10 ms and from 10 ms to 100 ms, respectively. For many rodlike micelles, the fourth relaxation time is close to the stress relaxation time determined by the rheological measurements.[72),76)] They considered that the second process comes from a coupled rotational translational motion and the third and the fourth processes are due to the orientational motion of rods and deformational motion of the entanglement networks, respectively. However the details of the second, third and fourth relaxation processes have not been clarified yet.[76)] One of the reasons for this is the difficulty in estimating thickness of the electric double layer in rodlike micelles.

Shikata *et al.*[73)] examined the mixtures of hexadecyltrimethylammonium bromide and sodium salicylate by the transient flow birefringence and viscoelasticity. They clarified that for the entanglement networks of rodlike micelles, the stress-optical law holds well under the shear rate below 3 s^{-1}. Under the shear rate above 3 s^{-1}, the time dependence of the orientation angle varied in a wavy fashion and this behavior was not completely reproducible and the stress-optical law no longer held. The wavy curve of flow birefringence was explained in terms of some drastic structural changes of the entanglement networks of micelles and also of the micelles themselves. This interpretation has not been proved by experiment. In flow birefringence, the shear rate is generally limited below 1000 s^{-1}. Information of birefringence under high shear rate or high frequency will help to elucidate the origin of the wavy curve of flow birefringence.

Compared with other birefringence methods, the advantages of the ultrasonically induced birefringence method are that it enables us to investigate the motion of rodlike micelles under flow of high frequency and it is free from the presence of ions or electric double layer of rodlike micelle. The purpose of this work is to investigate the dynamics of the entanglement networks of the rodlike micelles (hexadecyldimethylamine oxide: CDAO) and the rodlike micelles (mixtures of hexadecyltrimethylammonium bromide; CTAB and sodium salicylate; NaSal) by ultrasonically induced birefringence methods. The elastic property of the entanglement networks of the rodlike micelles will be discussed from the transient spectrum of ultrasonically induced birefringence.

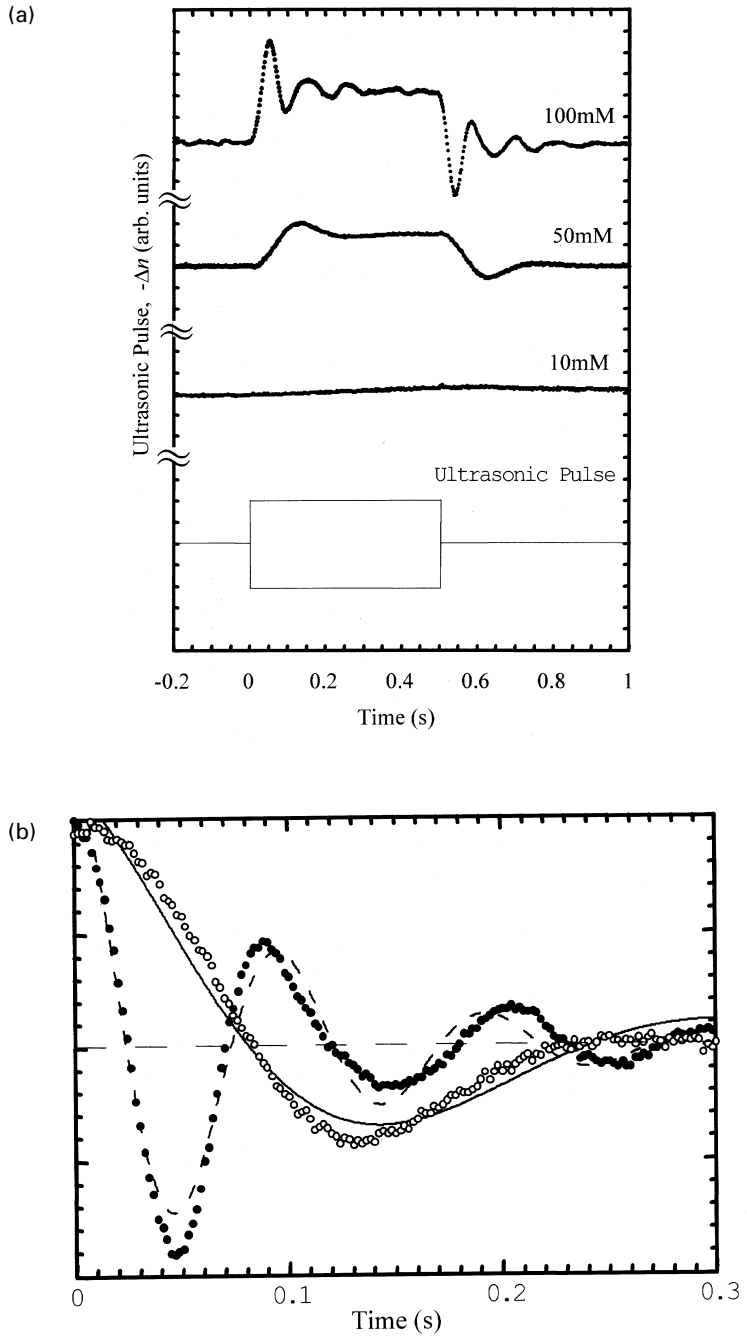

Fig. V-7 (a) Time dependence of the transient transmission light of 10, 50 and 100 mM CDAO at 35°C (25 MHz, 0.058 W/cm^2) and the waveform of the pulse used.
(b) Expanded illustration of the transient transmission light of CDAO after cessation of ultrasound. (●) 100 mM; (○) 50 mM. Dotted curve shows the calculated value with $I(t) = \exp(-t/0.09)\cos(2\pi t/0.10)$ Solid curve show the calculated value with $I(t) = \exp(-t/0.13)\cos(2\pi t/0.32)$

2) Birefringence of Rodlike Micelles

Figure V-7 (a) gives the ultrasonically induced birefringence measurements observed for 10, 50 and 100 mM CDAO and the waveform of the ultrasonic pulse used. A birefringence signal is not observed for 10 mM CDAO. The CDAO begins to form rodlike micelles above its critical micelle concentration (cmc = 2.5×10^{-5} M)[77] and the entanglement networks of the rodlike micelles are formed above about 20 mM.[78] The ultrasonically induced birefringence was observed for the entanglement networks.

The birefringence after the onset of ultrasound increases suddenly and approaches the steady value after a damped oscillation. The decay curve is expressed by as

$$\Delta n(t) = \Delta n_{st}(-t/\tau_d)\cos(2\pi t/T) \tag{V-16}$$

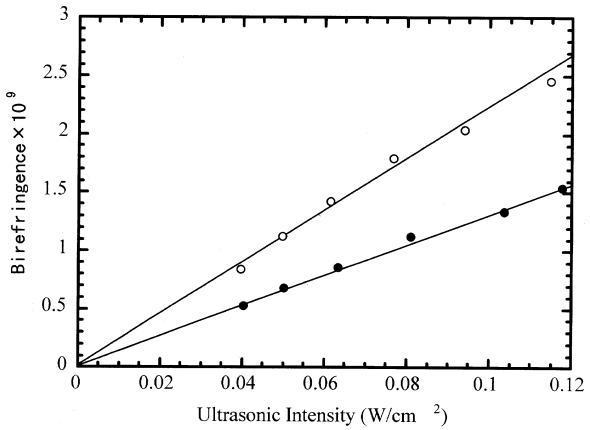

Fig. V-8 Birefringence of CDAO against ultrasonic intensity at 35°C (25 MHz): (○) 100 mM; (●) 50mM.

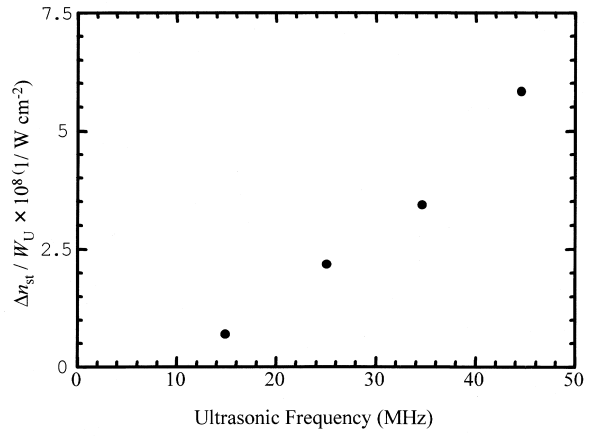

Fig. V-9 Frequency dependence of the birefringence for unit ultrasonic intensity at 100 mM CDAO.

where Δn_{st} is the birefringence at the stationary state, τ_d is the damping time constant and T is the period of oscillation. Figure V-7(b) indicates the time dependence of birefringence of 100 mM and 50 mM CDAO after the cessation of ultrasound. For both concentrations, the sign of the induced birefringence was negative. The value of Δn_{st} of 100 mM was 2.5×10^{-9}, while for 50 mM it was 1.5×10^{-9}.

Figure V-8 shows the birefringence of 50 and 100 mM CDAO as a function of the ultrasonic intensity. The birefringence is proportional to the ultrasonic intensity for both concentrations.

Figure V-9 refers to the frequency dependence of the birefringence of 100 mM CDAO normalized for ultrasonic intensity $\Delta n_{st}/W_U$. The $\Delta n_{st}/W_U$ increases with the frequency.

Ultrasonically induced birefringence was observed on the entanglement networks of rodlike micelles. The birefringence of the entanglement networks of the rodlike micelles was proportional to the ultrasonic intensity and increased with the ultrasonic frequency.

For solutions of flexible macromolecules, Peterlin[52),79)] gave a theory of the ultrasonically induced birefringence. According to the theory, the birefringence comes from the deformation of flexible macromolecules due to the velocity gradient of sound wave. Then the birefringence of flexible macromolecules is proportional to the square roots of ultrasonic intensity. As the birefringence of the rodlike micelles is proportional to the ultrasonic intensity, the birefringence is not interpreted in terms of the Peterlin theory. The birefringence for dilute solutions of rigid colloidal particles is formulated by Oka.[52),55)] If the ultrasonic frequency is much higher than the rodlike particle reorientational frequency, the radiation pressure due to the propagation of the sound wave causes the turning torque which aligns the minor axis of the particle to the direction of the ultrasonic wave propagation.[20)] Consequently, the birefringence of colloidal particles is proportional to the ultrasonic intensity. The ultrasonic intensity dependence of the birefringence of the entanglement networks indicates that the birefringence is induced by the radiation pressure. The frequency dependence of the birefringence results from the translational velocity difference between the entanglement networks and the solvent. With increasing ultrasonic frequency, the translational motion of entanglement networks with respect to solvent becomes more hindered. As the radiation pressure on the rodlike micelles increases with the translational velocity difference, the birefringence increases with the ultrasonic frequency.

3) Damped Oscillation Behavior of Transient Ultrasonically Induced Birefringence of the Rodlike Micelles

In Fig. V-7(b), the solid curve is the calculated one using Eq. (V-16) with τ_d = 0.09 s and T = 0.10 s for 100 mM of CDAO and the dotted curve is the calculated value with τ_d = 0.13 s and T = 0.32 s for 50 mM. These curves well reproduce the experimental results. The value of T increases with decreasing concentration, while the value of τ_d does not depend on the concentration of CDAO. It is interesting to note that the value of T of solutions of 50 mM CDAO is close to that of mixtures of 30 mM CDAO and 230 mM NaSal. Furthermore, it should be pointed out that the values of τ_d and T do not depend on both ultrasonic intensity and ultrasonic frequency.

No theory has been proposed yet which can explain the damped oscillation behavior of transient ultrasonically induced birefringence of the rodlike micelles. The viscoelastic properties[78),80),81)] of the entanglement networks of CDAO and the mixtures composed of CTAB and NaSal have been described by the Maxwell model which has only one stress relaxation time, τ_s, and the entanglement networks are regarded as elastic body with plateau modulus, G_0, at frequencies much higher than $1/\tau_s$. The shear stress[82)] on the entanglement networks of the mixtures of CTAB and NaSal exhibited the damped oscillation according as the start of shear flow of high rate above 0.24 s^{-1}. We considered the ultrasonically induced birefringence of rodlike micelles as follows. The entanglement networks suffer the stress due to the radiation pressure of the ultrasonic wave

Table V-1 Values of period T and Damping constant τ_d of a damped oscillation, the plateau modulus G_0, and the stress relaxaion time τ_s.

	mixtures of 30 mM CTAB and 230 mM NaSal	50 mM CDAO	100 mM CDAO
T/s	0.36	0.32	0.10
τ_d/s	0.28	0.13	0.09
G_0/Pa	4.4[a]	3.2[b]	10[c]
τ_s/s	2.5[a]	0.3[b]	0.3[c]

[a] Obtained at 25°C.[80] [b] Obtained at 60 mM.[82] [c] Ref. 82.

and shrink in the direction of sound propagation with damping elastic oscillation. In the shrinked entanglement network, the major axis of the rodlike micelles is elongated and orientated perpendicularly to the direction of the ultrasonic wave propagation. After the cessation of ultrasonic fields, the entanglement networks relax from a shrinked state with damping elastic oscillation. Since the fact that G_0 of the entanglement networks is approximately proportional to the square of the concentration of surfactant molecules is essentially equal to that observed in entangling polymer systems, for example, rubber,[80),83)] the period of damped oscillation of birefringence, T, is inversely proportional to the square root of G_0. The value of τ_d is the deformational relaxation time of the entanglement networks. Because τ_s comes from the movement of entanglement networks as a whole, the value of τ_d increases with τ_s.Table V-1 indicates τ_s and G_0, as well as τ_d and T. The value of T decreases with increasing G_0. Since the G_0 of 60 mM CDAO is comparable to the one of the mixtures of CTAB and NaSal, the value of T of 50 mM CDAO is close to the one of the mixtures of CTAB and NaSal. For CDAO, the both values of τ_s and τ_d are independent of concentration. The value of τ_d increases with the value of τ_s for CDAO and the mixtures of CTAB and NaSal. The quantitative relationships between G_0 and T and between τ_d and τ_s are not clear, since available data of τ_s and G_0 are few.

The sign of the birefringence depends on whether the orientational direction of major axis of the rodlike micelles is perpendicular or parallel to the propagation of sound wave and whether the birefringence is caused by the positive form birefringence of the rodlike micelles or the negative intrinsic birefringence of the surfactant monomers.[71)] In the ultrasonically induced birefringence measurements, the signs of birefringence were negative. The negative birefringence can be explained in two different ways. In one way the orientational direction of major axis of the rodlike micelles with the positive form birefringence of the rodlike micelles is perpendicular to the propagation of sound wave. In the other the orientational direction of major axis of the rodlike micelles with negative intrinsic birefringence of the surfactant monomers is parallel to the propagation of sound wave. The results of flow birefringence measurements[73)] show that the birefringence is caused by the negative intrinsic birefringence of the surfactant monomers. As described in the above section, the major axis of the rodlike micelles is elongated and orientated perpendicularly to the direction of ultrasonic wave propagation. The ultrasonically induced birefringence might be caused by the positive form birefringence of the rodlike micelles.

In order to study the rigidity of micelle and the salt dependences of damping oscillation of ultrasonically induced birefringence of rodlike micelles, we now are measuring the birefringence of rodlike micelles composed of the mixtures of CTAB and NaSal.

6. Ultrasonically Induced Birefringence in Polymer Solutions[84)]

Under the irradiation of longitudinal ultrasound, birefringence has been observed in some liquids and solutions of anisotropic solute molecules.[15),20),38)-43)] The mechanisms of the ultrasonically induced birefringence can be classified into two; one is by sinusoidal velocity gradient and the other is by ultrasonic radiation pressure.

In the normal neat liquids and solutions, reorientational relaxation times of molecules are almost equal in order or faster than ultrasonic frequency. Therefore, a reorientational motion of molecules can follow the sinusoidal velocity gradient produced by irradiation of ultrasonic waves and directly produces sinusoidal orientational order. The reorientational order produced is not uniform but propagates as waves and induces birefringence. In this case, the induced birefringence should be proportional to the ultrasonic amplitude, that is, the square root of the ultrasonic intensity[38),41)-43)] as shown in section IV (mechanism I).

On the contrary, for large particles of anisotropic shape such as rod like and planar colloidal particles, ultrasonic radiation pressure produces a stationary torque on the particles and induces reorientational order as a whole, because the orientational relaxation frequency of particles is much smaller than that of ultrasound frequency. In this case, the induced birefringence is proportional to the ultrasonic intensity.[15),20),38)-40)] as expressed by Oka[55)] and Ou-Yang[15)] theories (mechanism II). Furthermore, the dynamical properties of large particles can be investigated by following the decay of the birefringence after rapid cessation of ultrasonic irradiation.[15),20),38)-40)]

As shown in the experimental session, in order to measure the ultrasonically induced birefringence, used following two methods. One was the method in which the $\lambda/4$ plate is set in the optical path (biased detection) and the other was the method without $\lambda/4$ plate(non-biased detection) (see section II). In every case, ultrasonically induced birefringence Δn can be expressed by Eqs. (II-6) and (II-7), respectively.

Ultrasonically induced birefringence caused by mechanism I changes periodically following the phase change of the ultrasonic wave in space and time. Taking into consideration of the radius of the laser bean and cut-off frequency of the optical detector, the birefringence signal should be zero by averaging in the biased detection. Therefore, the biased detection can only detect the birefringence caused by mechanism II. By the non-biased detection, the root mean square of the birefringence signal can be observed. So, the birefringence caused by both mechanisms will be measured.

It is well known that flow birefringence can be observed in polymer solution under the stationary shear stress.[85)] As shown in section IV, the ultrasonically induced birefringence should be also observed in polymer solutions. As expected, ultrasonically induced birefringence has been observed in polystyrene toluene and polyisobutylene cyclohexane solutions by Jerrard.[14)]

For ultrasonically induced birefringence, Peterlin has proposed a theory for flexible macromolecules.[78)] He considered that the polymer solution will behave more as a liquid than a colloidal solutions, because of the flexibility of the molecules in which he considered to be permeable spheres in which the solvent was partially in immobilized. The optical behavior was calculated as for a liquid by finding an expression for the mean polarizabilitites in two direction and using the method of Langevin to connect the anisotropy of the polarizability to the birefringence.

To relate the difference in the polarizabilities to the geometrical parameters of the molecules, Peterlin used the Kuhn model,[86)] namely a random coil, composed of the number of N_m segments, having the mean length A_m and the end-to-end distance equal to h. The distribution in h is considered to rise from a kinetic equilibrium between a statistical force tending to contract the chain to the most probable value of h and a force due to the thermal motion which is dependent on the rotary and internal diffusion constant D_i of molecules. Under the influence of the acoustic field, he consedered the spherically shaped molecule to be deformed to give a new distribution in h from

which the anisotropy of the polarizability may be calculated.

If V_{rel} is the velocity, the distribution function of F finding the value of h is given by the following diffusion equation:

$$\mathrm{div}\,[V_{rel} \cdot F - D_c\,(2\mu hF + \mathrm{grad}\,F)] = -\partial F/\partial t \qquad \text{(V-17)}$$

where $\mu = 3/2N_mA_m^2$ and D_c is a diffusion constant which is not only a function of rotary diffusion constant D and but also is a function of D_i.

Peterlin used the results of Kuhn and Grun[87] in which they regarded each segment (that is, straight chain element) as being optical anisotropic with polarizabilities α_1 and α_2 along and perpendicular to its axis. Considering the whole molecule they found the mean polarizabilities γ_1 and γ_2 in direction along and perpendicular to the segment h. For the values of h smaller than the total chain length, they give

$$\gamma_1 - \gamma_2 = (\mu h^2)(\alpha_1 - \alpha_2)/15 \qquad \text{(V-18)}$$

The contribution to the polarizability of the whole medium by each molecule depends not only on the magnitude of h but also on its orientation. The total contribution of all the molecules is therefore determined using the distribution function F given by the solution of Eq. (V-17).

According to the consideration mensioned above, Peterlin obtained the following expression for ultrasonically induced birefringence of polymer solutions.

$$\Delta n_{rms} = 2\pi n \eta_0\, c[M]_{sp}\, f\left(\frac{W_U}{\rho v^2}\right)^{1/2} \frac{1}{(1+\omega^2\tau^2)^{1/2}} \qquad \text{(V-19)}$$

where, $\tau = 1/4\,\mu D$, n is the refractive index of the solution, η_0 is the solvent shear viscosity, c is the concentration in g/cm^3, $[M]_{sp}$ is a specific Maxwell constant, f is the frequency and $\omega = 2\pi f$. This equation resembles the Eq. (IV-31) which Peterlin gives for neat liquids.[54]

Jerrard measured the ultrasonically induced birefringence of polystyrene-toluene and polyisobutylene-cyclohexane solution as a function of ultrasonic intensity and frequency (1–6 MHz). His experimental set up corresponds to the non-biased detection in our system. He has reported that ultrasonically induced birefringence of polymer solutions is proportional to the square root of the irradiated ultrasonic intensity.

In the ultrasonic frequency region from several MHz to GHz, the ultrasonic relaxation processes which arise from the local segmental motion have been observed. As is seen in Eq. (V-17), in the case of the polymer solutions, the mechanisms of the birefringence will be more complicated than in pure liquids and colloidal suspensions. The torque which comes from the ultrasonic irradiation pressure will couple with the local segmental motions of polymer chains in solution.

In order to clarify the birefringence mechanisms, we measured the ultrasonically induced birefringence of polystyrene-tolune solutions using both biased and non-biased measurement. The birefringence of polymer solutions has been obtained by both biased and non-biased measurement. Typical birefringence signal obtained by the biased measurement is shown Fig. V-10. As shown in Fig. V-10, the rise and decay times of the ultrasonically induced birefringence signals are almost same as that ultrasonic pulse as 5 μs. These results also obtained by the non-biased detection. The sign of the birefringence signal can be determined by the biased detection. In this work, the sign was positive. Figure V-11 shows the ultrasonic irradiation intensity dependence of birefringence. As is seen in Fig. V-11, birefringeces observed by the non-biased detection are in proportional to

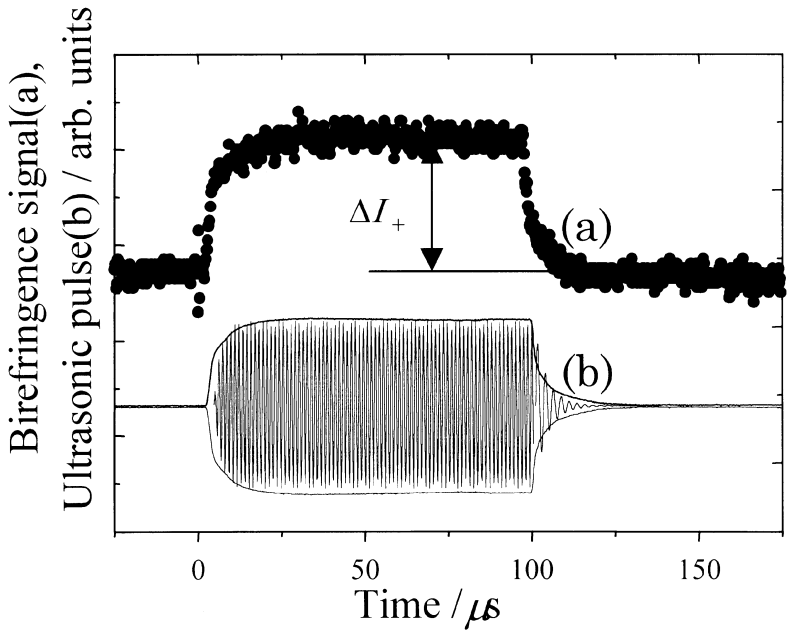

Fig. V-10 Birefringence signal of polystyrene-toluene solution using a quarter wave plate. (10 wt%, 25 MHz, 25°C).

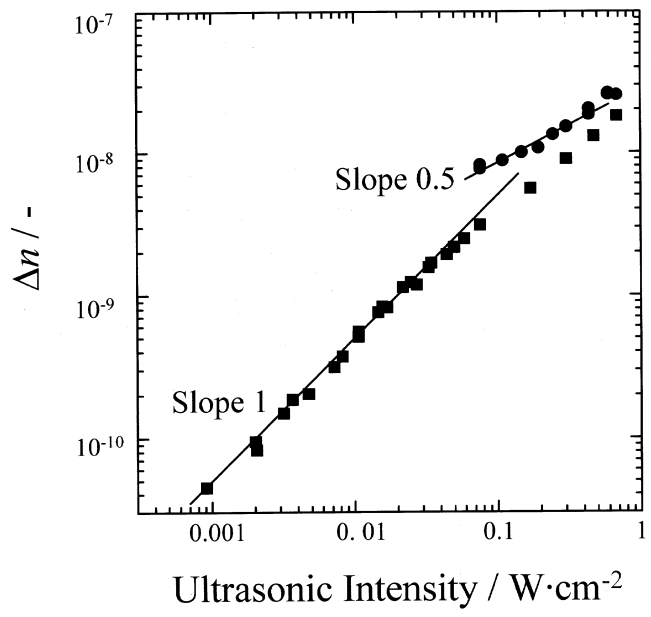

Fig. V-11 Utrasonic intensity dependence of birefringence in polystyrene-toluene solution (10 wt%, 25 MHz, 25°C). (■: with quarter wave plate, ●: without quarter waveplate)

the square the root of the ultrasonic intensity, but those obtained by the biased detection are in linearly proportional to the ultrasonic intensity. The values of the birefringence signal measured by the biased detection are smaller than those obtained by the non-biased detection at all ultrasonic intensities. The experimental results for the parts which were proportional to the square root of the ultrasonic intensity are in agreement with those obtained by Jerrard for polystyrene-toluene solutions. However, the parts which are linearly proportional to the ultrasonic intensity was not reported and the result obtained in our work is the first case.

It is very interesting that in the polymer solutions, at fairly strong region of the ultrasonic power, two kinds of ultrasonically induced birefringence were clearly observed. The birefringence obtained by the non-biased detection, that is, part proportional to the square root of the ultrasonic power will be caused by sinusoidal velocity gradient which was obtained by Jerrard. The parts of birefringence obtained by the biased detection were clearly measured even in the low ultrasonic intensity region and linearly proportional to the ultrasonic intensity.

As well known, in polymer solutions, the typical non-linear viscoelastic behavior, that is the stress normal mode effects, has been observed. Badoz[88)] has modified the Peterlin's theory for macromolecular solution to take into account the elastic effects of polymer chains in solutions. The expression of birefringence obtained from this elastic model also indicates that the values of birefringence are linearly proportional to the ultrasonic frequency and square root of the ultrasonic intensity.

The frequency dependence of the birefringence of polymer solutions will be very important. Our work on this line is now going on.

For the ultrasonically induced birefringence measurement of polymer solutions, it is very interesting and very important that the two different types of birefringence were observed. In order to elucidate the detailed mechanisms of polymer chain motions in solutions ultrasonically induced birefringence measurement has opened a new field of the chain dynamics. In this case, the key factor is how the translational and rotational motion of molecules couples with each other.

VI. General Conclusion and Scope

In this review, we discussed the coupling between translational and rotational motion of liquid crystal molecules in isotropic phase as an example of liquids. The coupling parameter R obtained from the depolarized light scattering measurements is an important parameter to deduce the information about the relation between the anisotropic molecular interaction and the local structure of liquids and solutions. Besides, we presented a theory of the ultrasonically induced birefringence in neat liquids and discussed the problem of coupling between the reorientational (rotational) mode and longitudinal mode. Our theory is not agreement with that of the irreversible statistical mechanics. The longitudinal mode is described as the sum of the bulk and shear mode. The discrepancy between our theory and that of the irreversible statistical mechanics comes from the difference in the choice of the coupled variables. In order to clarify this point, we must consider how the molecular volume and the rotational motion correlate each other in molecular level. For the ultrasonically induced birefringence measurement, two type of birefringence were observed; one is proportional to the square root of ultrasonic intensity and the other the ultrasonic intensity itself.

It is well known that in liquids such as benzene and their derivatives, the reorientational relaxation times τ can be expressed $\tau = C\eta + \tau_{00}$ as a function of translational viscosity η, where C is a constant and τ_{00} is a time constant which is correlated with the classical "free-rotator reorientation" time.[1)] The value of constant C has been discussed in their relation to the boundary condition, that is "stick" or "slip" boundary one. The similar kinds of discussion also have been made on the

translational diffusion constant. However translational and rotational diffusion coefficients should be expressed in terms of molecular interaction potentials. In the molecular level or in a very short range region, the translational and rotational motion should be coupled each other. We are obliged to discuss the interaction between the translational and rotational motions as a measure of hydrodynamic parameter *C* because of the lack of the information about the interaction between the translational and rotational motions in the molecular level.

The problems such as the coupling parameter *R* and ultrasonically induced birefringence discussed in the review are related directly to how the molecular interaction potential of the atom and atoms reflects on the molecular motion in the molecular level and also what the molecular volume is. Thus, the molecular interactions in the molecular and very short range levels even in the static and dynamic meanings are essential. However, a limitted number of experimental techniques are available to obtain the information about the coupling of the translational and rotational motions. The techniques available are only depolarized light scattering and flow and ultrasonically induced birefringences.

We remember the following Einstein's messages;
"Raffiniert ist der Herrgott aber boshaft ist er nicht."
"Die Natur verbirgt ihr Geheimnis durch die Erhabenheit ihres Wesens, aber nicht durch List."

References

1) B. Berne and R. Pecora, *Dynamic Light Scattering*, (New York, Wiley, 1976).
2) D. Kivelson and P. A. Madden, Ann. Rev. Phys. Chem. **31**, 523 (1980) and references therein.
3) P. G. de Gennes, Mol. Cryst. Liq. Cryst., **12**, 193 (1971).
4) T. D. Gierke and W. H. Flygare, J. Chem., Phys., **61**, 2231 (1974).
5) C. Filippini and Y. Poggi, Phys. Lett., **65A**, 30 (1978) and reference therein.
6) P. Martinoty, S. Candau and F. Debeauvais, Phys. Rev. Lett., **27**, 1123 (1971).
7) Y. Kawamura, PhD thesis, University of Tokyo, 1982; Y. Kawamura and S. Iwayanagi, Mol. Cryst. Liq. Cryst., **38**, 239 (1977).
8) S. J. Tsay and D. Kivelson, Mol. Phys., **29**, 1 (1975).
9) H. C. Anderson and R. Pecora, J. Chem. Phys., **54**, 2584 (1971).
10) T. Keys and D. Kivelson, J. Chem. Phys., **54**, 1786 (1971), and **56**, 1876 (1972).
11) G. R. Alms D. R. Bauer, J. I. Brauman and R. Pecora, J. Chem. Phys., **59**, 5304 (1973).
12) R. Lipeles and D. Kivelson, J. Chem. Phys., **72**, 6199 (1980).
13) J. L. Viovy G. M. Searby, P. Sixou and J. V. Champion, Mol. Phys., **39**, 471 (1980).
14) H. G. Jerrard, Ultrasonics, **2**, 74 (1964).
15) H. D. Ou-Yang,. R. A. MacPhail and D. Kivelson, Phys. Rev., **A33**, 611 (1986).
16) S. Koda, T. Koyama,Y. Enomoto and H. Nomura, Jpn. J. Appl. Phys., **31**, Suppl.31-1, 51 (1992).
17) T. Shibata, T. Matsuoka, S. Koda and H. Nomura, J. Chem. Phys., **109**, 2038 (1998).
18) T. Matsuoka, K. Sakai and K. Takagi, Phys. Rev. Lett., **71**, 1510 (1993).
19) T. Matsuoka, K. Sakai and K. Takagi, Rev. Sci. Instrum., **64**, 2136 (1993).
20) K. Yasuda, T. Matsuoka, S. Koda and H. Nomura, J. Phys. Chem., **100**, 5892 (1996).
21) T. Matsuoka, K. Yasuda, S. Koda and H. Nomura, J. Chem. Phys., **11**, 1580 (1999).
22) W. R. Klein and B. D. Cook, IEEE Trans. Sonics. Ultrason., **SU-14**, 123 (1967).
23) R. B. Gibson and Kinkaid, J. Am. Chem. Soc., **60**, 511 (1938).
24) S. M. Rytov, Zh. Eksp. Teor. Fiz., **33**, 514 (1957).
25) G. I. A. Stegeman and B. P. Stoicheff, Phys. Rev. Lett., **21**, 202 (1968); Phys. Rev., **A7**, 1160 (1973).
26) W. Lempert and C. H. Wang, J. Chem. Phys., **72**, 3490 (1980).
27) G. R. Alms, T. D. Gierke and G. D. Patterson, J. Chem. Phys., **67**, 5779 (1977).
28) T. Ueno, K. Sakai and K. Takagi, Phys. Rev. E, **54**, 6457 (1996).

29) T. Shibata, T. Matsuoka, S. Koda and H. Nomura, Jpn. J. Appl., **38**, 2059 (1999).
30) T. Shibata, T. Matsuoka, S. Koda and H. Nomura, J. Mol. Liq., in press.
31) S. L. Whittenburg and C. H. Wang, J. Chem. Phys. **66**, 4995 (1977).
32) P. J. Chappell and D. Kivelson, J. Chem., Phys., **76**, 1742 (1982).
33) G. K. L. Wong and Y. R. Shen, Phys. Rev., A, **10**, 1277 (1974).
34) J. D. Lister and T. W. Stinson III, J. Appl. Phys., **41**, 996 (1970).
35) G. R. Alms and G. D. Patterson, J. Chem. Phys., **68**, 3440 (1978).
36) J. Leadetter, R. M. Richardson, and C. N. Colling, J. Phys. (Paris), **36**, C1-37 (1975).
37) G. W. Gray and A. Mosley, Mol. Cryst. Liq. Cryst., **35**, 72 (1976).
38) H. G. Jerrard, Ultrasonics, **2**, 74 (1964).
39) K. Yasuda, T. Matsuoka, S. Koda and H. Nomura, Jpn. J. Appl. Phys., **33**, 2901 (1994).
40) K. Yasuda, T. Matsuoka, S. Koda and H. Nomura, J. Phys. Chem. B, **101**, 1138 (1997).
41) P. Martinoty and M. Bader, J. Phys. (Paris), **42**, 1097 (1981).
42) M. Bader and P. Martinoty, Mol. Cryst. Liq. Cryst., **76**, 269 (1981).
43) P. G de Gennes and J. Prost, *The Physics of Liquid Crystals 2nd ed.* (Clarendon, Oxford, 1993), Chap. 2.
44) P. Martinoty, F. Kiry, S. Nagai and S. Candau, J. Phys. (Paris), **38**, 159 (1977).
45) D. Kivelson and T. Keyes, J. Champion, Mol. Phys., **31**, 221 (1976).
46) P. J. Chappell, M. P. Allen, R. I. Hallem and D. Kivelson, J. Chem. Phys., **74**, 5929 (1981).
47) M. P. Allen, P. J. Chappell and D. Kivelson, J. Chem. Phys., **74**, 5942 (1981).
48) R. Lipeles and D. Kivelson, J. Chem. Phys., **67**, 4564 (1977).
49) W. T. Grubbs and R. A. MacPhail, J. Chem. Phys., **97**, 8906 (1992).
50) C. H. Wang, Mol. Phys., **58**, 497 (1986).
51) J. Frenkel, *Kinetic Theory of Liquids*, (Clarenden, Oxdord, 1946), Chap. 5.
52) N. C. Hilyard and H. G. Jerrard, J. Appl. Phys., **33**, 3470 (1962).
53) Peterlin, J. Phys. Radium, **11**, 45 (1950).
54) H. Kawamura, Kagaku (Tokyo), **7**, 6 (1938); **7**, 54 (1938); **7**, 139 (1938) [in Japanese].
55) S. Oka, Kolloid Z., **87**, 37 (1939); Z. Physik., **116**, 632 (1940).
56) S. Petralia, *Nuovo Cimento*, **17**, 378 (1940).
57) T. Yasunaga, N. Tatsumoto and H. Inoue,. J. Colloid & Interface Sci., **29**, 178 (1969).
58) P. Debye, P. *Polar molecules*, (Dover, New York, 1929).
59) R. Polhman, *Z Physik.*, **107**, 497 (1937).
60) L. V. King, Proc Roy. Soc. London ser., **A153**, 1 (1935); **A153**, 17 (1935).
61) J. W. S. Rayleigh, *Theory of Sound, 2nd ed.*, (Dover, New York, 1945).
62) W. König, Wied. Ann t., XXXII, 43, (1891).
63) A. Peterlin and H. A. Stuart, Z. Physik, **112**, 129 (1939).
64) L. D. Landau and P. M. Lifshitz, *Fluid Mechanics*, (Pergamon Press, Oxford, 1959).
65) S. H. Lamb, *Hydrodynamics* 6th ed., (Cambridge at the University Press, 1932).
66) F. Perrin, J. Phys. & Rad., **5**, 197 (1934); **7**, 1 (1936).
67) M. Ozaki, S. Kratohvil and E. Matijevic, J. Colloid & Interface Sci., **102**, 146 (1984).
68) R. O. James, Colloids Surfaces, **27**, 133 (1987).
69) H. Hoffmann, G. Oetter and B. Schwandner, Prog. Colloid Polym. Sci., **72**, 95 (1987); **73**, 95 (1987).
70) H. Pilsl, H. Hoffmann, S. Hofmann, J.Kalus, A. W. Kencono, P. Lindner and W. Ulbricht, J. Phys. Chem., **97**, 2745 (1993).
71) H. Rehage and H. Hoffmann, J. Phys. Chem., **92**, 4712 (1988).
72) H. Hoffmann, U. Kramer and H.Thurn, J. Phys. Chem., **94**, 2027 (1990).
73) T. Shikata, S. J. Dahman and D. S. Pearson, Langmuir, **10**, 3470 (1994).
74) S. Hofmann, A. Rauscher and H. Hoffmann, Ber. Bunsenges. Phys. Chem., **95**, 153 (1991).
75) Y. Hu, S. Q. Wang and A. M. Jamieson, J. Colloid Interface Sci., **156**, 31 (1993).
76) H. Hoffmann, A. Rauscher, M. Gradzielski and S. F.Schulz, Langmuir, **8**, 2140 (1992).
77) G. Platz, C. Thunig and H. Hoffmann, Prog. Colloid Polym. Sci., **83**, 167 (1990).
78) K. Hashimoto and T. Imae, Langumir, **7**, 1734 (1991).
79) A. Peterlin, Rec. trav. Chim., **69**, 14 (1950).
80) T. Shikata and T. Kotaka, J. Non-Crystalline Solids, **131–133**, 831 (1991).

81) E. K. Wheeler, P. Izu and G. G.Fuller, Rheol. Acta, **35**, 139 (1996).
82) T. Shikata, H. Hirata, E. Takatori and K. Osaki, Non-Newtonian Fluid Mech., **28**, 171 (1988).
83) T. Shikata, private communication.
84) T. Matsuoka, S. Koda and H. Nomura, Jpn. J. Appl. Phys., **39**, (2000) to be published.
85) M. Doi and S. F. Edwards, *The Theory of polymer Dynamics*, Clarendon Press, Oxford, (1986).
86) W. Kuhn, Kolloid-Z., **68**, 2 (1934); Z-angew Chem., **49**, 858 (1936); Experientia **1**, 28 (1945).
87) W. Kuhn and F. Grun, Kolloid-Z., **101**, 248 (1942).
88) J. Badoz, J. Phys. Radium, **15**, 777 (1954).